JGR Atmospheres

RESEARCH ARTICLE
10.1029/2025JD044117

# The Memories of Soil Moisture and Soil Temperature Anomalies in Subsequent Soil Moisture and Soil Temperature in China

**Yaoming Song[1,2], Haishan Chen[1,2], Lin Wang[1,3], Anning Huang[4], and Wei Gu[5]**

[1]State Key Laboratory of Climate System Prediction and Risk Management/Key Laboratory of Meteorological Disaster, Ministry of Education/Collaborative Innovation Center on Forecast and Evaluation of Meteorological Disasters, Nanjing University of Information Science and Technology, Nanjing, China, [2]School of Atmospheric Sciences, Nanjing University of Information Science and Technology, Nanjing, China, [3]Center for Monsoon System Research, Institute of Atmospheric Physics, Chinese Academy of Sciences, Beijing, China, [4]School of Atmospheric Sciences, Nanjing University, Nanjing, China, [5]Laboratory for Climate Studies, National Climate Center, China Meteorological Administration, Beijing, China

**Key Points:**

- The study presents a Lagrangian-based understanding of soil moisture and soil temperature memories
- The memories are longer in the northern part of China and the Qinghai-Tibet Plateau than in the rest of China
- The memories of soil moisture anomalies are longer in frozen soil, non-flood season and the arid-humid transition zone

**Supporting Information:**

Supporting Information may be found in the online version of this article.

**Correspondence to:**

Y. Song,
songym@nuist.edu.cn

**Citation:**

Song, Y., Chen, H., Wang, L., Huang, A., & Gu, W. (2026). The memories of soil moisture and soil temperature anomalies in subsequent soil moisture and soil temperature in China. *Journal of Geophysical Research: Atmospheres*, *131*, e2025JD044117. https://doi.org/10.1029/2025JD044117

Received 16 APR 2025
Accepted 29 DEC 2025

**Abstract** The memories of soil moisture (SM) and soil temperature (ST) modulate the effect of land surface on climate prediction on monthly and longer timescales. Based on a Lagrangian-based understanding of SM and ST memories, this study explores the characteristics of SM and ST memories using ERA5-Land reanalysis data, observations, land surface model and WRF model. The results show that SM and ST memories are longer in North China, Northeast China, Northwest China and Qinghai-Tibet Plateau than in other regions of China, even exceeding 10 months. In the southern part of China, memories are short, approximately 0–6 months. SM memories have similar spatial distributions at different soil depths over 12 months, as do ST memories. The WRF-simulated memories show generally consistent spatial patterns with ERA5-Land but are lower in some regions. Moreover, SM and ST anomalies mainly persist in the form of subsequent SM and ST anomalies, respectively. The relationships between the memories and land surface fluxes exhibit distinct characteristics in arid and wet regions. The memories of SM anomalies are longer in frozen soil, non-flood season and the arid-humid transition zone. Additionally, SM and ST memories are characterized with clear monthly and decadal variations, which may be related to some oceanic and atmospheric patterns. This study advances the understanding of critical processes linking land conditions before a certain time to atmosphere thereafter.

**Plain Language Summary** Climate prediction signals originate primarily from land surface and ocean processes. Soil moisture (SM) and soil temperature (ST) are key factors in land-atmosphere interactions, and the memories of SM and ST anomalies can modulate the effect of land surface on climate prediction. Based on the Lagrangian perspective, this study explores the temporal and spatial characteristics of the SM and ST memories and their relationships with climate indices and land surface fluxes in China. The results show that SM and ST memories are longer in North China, Northeast China, Northwest China and Qinghai-Tibet Plateau than in other regions of China, even exceeding 10 months. In the southern part of China, memories are short, approximately 0–6 months. The connections between the memories and land surface factors work differently in dry areas compared to rainy regions. SM anomalies last longer in frozen ground, non-flood periods, and the transitional zones between arid and humid regions. SM and ST variations show monthly and 10-year cycles that may connect to larger climate patterns. The study is meaningful for understanding the role and potential of land surface in climate prediction.

## 1. Introduction

Due to the chaotic nature of the atmosphere, the anomalies of atmospheric variables can only persist for a short time (Lorenz, 1969); therefore, climate prediction signals on monthly to decadal scales come mainly from land surface and ocean (Mariotti et al., 2018). As an important component of climate system, land surface affects climate change through land-atmosphere interactions. Soil moisture (SM) and soil temperature (ST) are key land surface variables in land-atmosphere interactions. The persistence of the SM and ST anomalies, also called memory, modulates the impact of land surface on climate change (Benson & Dirmeyer et al., 2023; Liu et al., 2014; Xue et al., 2018; Yang et al., 2019).

Numerous studies have confirmed the influences of SM and ST on subsequent atmospheric variables on monthly and longer timescales (Dong et al., 2022; Mahanama et al., 2008; Tang et al., 1987; Wang et al., 2013; Xue et al., 2018), and these studies mainly focus on the influence of spring ST (Mahanama et al., 2008; Tang et al., 1987; Wang et al., 2013; Xue et al., 2018; Yang et al., 2019, 2021, 2022; Zhang et al., 2018) or spring SM (Dong et al., 2022; Gao et al., 2019, 2020; Ma et al., 2018; Zhu et al., 2021) on subsequent atmosphere. Because the anomalies of SM and ST have longer memory than atmospheric anomalies, the persistence of ST and SM anomalies is crucially responsible for SM and ST influences on the subsequent atmosphere. Observational analysis and numerical simulations show that SM and ST anomalies can persist from weeks, seasons to longer time (Amenu et al., 2005; Entin et al., 2000; Hsu et al., 2017; Hu & Feng, 2004; Koster & Suarez, 2001; Kumar et al., 2019; Li et al., 2020; Lin et al., 2022; Liu & Avissar, 1999; Liu et al., 2014; Qiu et al., 2021; Seneviratne et al., 2006; Song et al., 2019, 2022a, 2022b; Vinnikov et al., 1996; Wu & Dickinson, 2004; Yang & Dominguez, 2019; Yang & Zhang, 2016). The processes affecting SM and ST memories are very complex, and some studies have confirmed the important role of soil texture (Liu et al., 2020; Song et al., 2019), soil column depth (Liu et al., 2020), freeze-thaw process (Li et al., 2021; Schaefer et al., 2007) in SM and ST memories.

SM and ST affect subsequent atmosphere through two processes. The first process is the persistence of antecedent SM and ST anomalies, and the second process is the influence of subsequent SM and ST anomalies on subsequent atmosphere through land-atmosphere interactions (Kumar et al., 2019; Li et al., 2021; Liu et al., 2020; Schaefer et al., 2007; Song et al., 2023). The memory of SM anomalies (SMM) and the memory of ST anomalies (STM) establish the connection among the antecedent SM and ST, current SM and ST, and current atmosphere. The anomalies of ST and SM can lead to the anomalies of other variables in soil, such as subsequent ST anomalies caused by SM anomalies; therefore, the anomaly signals of any variables in the soil caused by SM or ST anomalies need to be considered in the calculation of SMM or STM, and the anomaly signals may be from different variables at different soil depths. Complementing traditional Eulerian-based approaches (Amenu et al., 2005; Hu & Feng, 2004; Li et al., 2020; Wu & Dickinson, 2004; Yang & Zhang, 2016), this study introduces a Lagrangian perspective to calculate the memories of SM and ST. In traditional Eulerian-based understanding, SMM is calculated based on the relationships between current and subsequent SM in a fixed soil layer. But SM anomalies may lead to subsequent ST anomalies, and vice versa. In other words, both subsequent SM and ST anomalies need to be considered in the calculation of SMM, which are not considered in traditional Eulerian-based understanding. The calculation for STM should also be based on the same understanding. Moreover, the ST anomaly signals in a given soil layer can propagate to other layers, leading to subsequent ST and SM anomalies in other layers, which is a physical process related to STM. However, this is not adequately taken into account in the calculation for STM using traditional understanding. Furthermore, there also is a lack of systematic and comprehensive understanding of the memories of ST and SM anomalies in China (Li et al., 2020; Yang & Zhang, 2016). Based on the above, the main questions are as follows: What are the spatial distributions and temporal variations of STM and SMM in China during the past 40 years? And how do the anomalies of ST and SM propagate temporally to affect subsequent ST and SM across monthly to multi-year timescales? What might be the atmospheric factors affecting the spatial distributions and temporal variations of STM and SMM in China?

## 2. Data and Methods

### 2.1. Data

The data used in this study are from the ERA5 and ERA5-Land (ERA5L) reanalysis data sets (Hersbach et al., 2023a, 2023b), and the variables include monthly precipitation, evaporation, 2-m air temperature (T2m), ST and SM in four soil layers. The four soil layers are from 0 to 7 cm, from 7 to 28 cm, from 28 to 100 cm and from 100 to 289 cm, respectively. The above data are from 1979 through 2023. For more information about the data, refer to the ERA5 website: http://apps.ecmwf.int/data-catalogues/era5. ERA5 assimilates weather site data, numerical weather forecasts and satellite observations, and is more accurate and covers a longer time than previous versions (Zhang et al., 2023). Moreover, ST observation data in seven soil layers at 2,479 sites spanning from 1960 to 2013 are provided by the China Meteorological Administration (CMA), and the seven soil layers includes 0.05, 0.10, 0.20, 0.40, 0.80, 1.60 and 3.20 m. SM observation data at depths of 0.1 and 0.2 m across 778 sites spanning from 1991 to 2010 are also provided by the CMA. Daily precipitation and T2m observation data are from National Centers for Environmental Information (https://www.ncei.noaa.gov/maps/daily).

### 2.2. Methods

STM and SMM are the key processes that connect antecedent SM and ST, current SM and ST, and current atmosphere. To better quantify the persistence of ST/SM anomaly signals in soil, the statistical relationships between ST/SM and subsequent ST and SM were analyzed using ERA5L data and Pearson correlation coefficient. The correlation between ST and subsequent ST indicates the projection of the ST onto the subsequent ST. Using the ERA5L data, Pearson correlation coefficients between the ST of the first soil layer for 12 months from January to December and the subsequent ST/SM in different soil layers were calculated. Similar calculations were also performed for the ST in the other soil layers. Moreover, a similar analytical approach was applied to SM. The results presented in Section 3 show ST anomalies can affect subsequent ST and SM, and the same holds true for SM anomalies.

In land surface processes, the changes of some variables follow a natural exponential or a natural logarithmic relationship over time and with soil depth. These variables include saturated hydraulic conductivity (Beven & Kirkby, 1979; Sivapalan et al., 1987), subsurface runoff (Niu et al., 2005) and the decay of SM anomalies (Delworth & Manabe, 1988; Jones, 1975; Song et al., 2019). The variations of ST and SM are closely related to hydraulic conductivity, subsurface runoff, the decay of SM anomalies and other factors. Therefore, the changes of anomaly signals of ST and SM over time and with soil depth may follow natural exponential functions or natural logarithmic functions. To further confirm the functional form corresponding to the changes of the intensity of ST and SM anomaly signals over time, and the characteristics of the propagation of ST and SM anomaly signals in subsequent ST and SM, some numerical experiments were performed using a land surface model. Using the Community Land Model version 4.5 (CLM4.5) (Oleson et al., 2013), the preliminary numerical experiments show that the temporal variation of the intensity of ST and SM anomaly signals caused by the initial ST or SM anomalies is a natural logarithmic function of lag time, as is that of the soil depth where the strongest anomaly signals are located (Section 3). Therefore, natural logarithmic functions are used to analyze STM and SMM in this study.

Additionally, to better understand the functions describing SM and ST variations with depth and time, and to strengthen the theoretical foundation of this study, with ST as an example, a derivation under a set of idealized conditions was conducted. The logarithmic or exponential relationship can also be obtained under the assumption that heat capacity, thermal conductivity and hydraulic conductivity are constants. Taking the soil heat balance equation as an example:

Taking a soil block as an example, and the length, width, and height are $\Delta x$, $\Delta y$, and $\Delta z$, respectively, and the volume is $\Delta \tau$. $I$ is the internal energy of the soil block, and the heat balance equation is:

$$\Delta I = \left(\frac{\partial}{\partial x}\left(\kappa_x \frac{\partial T}{\partial x}\right) + \frac{\partial}{\partial y}\left(\kappa_y \frac{\partial T}{\partial y}\right) + \frac{\partial}{\partial z}\left(\kappa_z \frac{\partial T}{\partial z}\right)\right)\Delta\tau \tag{1}$$

$\kappa$ is the thermal conductivity of the soil.

$\frac{\Delta I}{\Delta \tau} \propto \frac{\partial C_v T}{\partial t}$ is the rate of change of internal energy per unit volume of the soil over time, $C_v$ is the volumetric heat capacity of the soil at constant volume, $T$ is soil temperature.

$$\frac{\partial C_v T}{\partial t} = \frac{\partial}{\partial x}\left(\kappa_x \frac{\partial T}{\partial x}\right) + \frac{\partial}{\partial y}\left(\kappa_y \frac{\partial T}{\partial y}\right) + \frac{\partial}{\partial z}\left(\kappa_z \frac{\partial T}{\partial z}\right) \tag{2}$$

For the vertical one-dimensional condition, if we further assume that $C_v$ and $\kappa_z$ are constants, then the heat conduction equation can be simplified as:

$$C_v \frac{\partial T}{\partial t} = \kappa_z \frac{\partial^2 T}{\partial z^2} \tag{3}$$

The solution to the above equation can be obtained as:

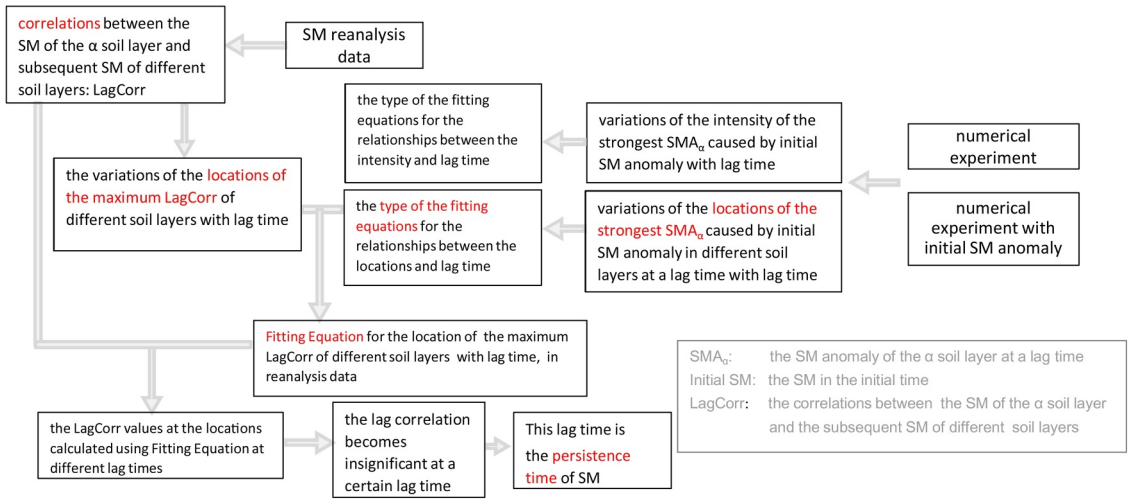


**Figure 1.** Flowchart for calculating Persis_SM_SM, which is the persistence of SM anomaly signals in subsequent SM.

$$T(z,t) = C_1 \exp\left(\frac{c_2}{c_v}t \pm \sqrt{\frac{c_2}{\kappa_z}}z\right) \tag{4}$$

$$\frac{\partial T}{\partial t} = \frac{c_1 c_2}{c_v}\exp\left(\frac{c_2}{c_v}t \pm \sqrt{\frac{c_2}{\kappa_z}}z\right) \tag{5}$$

$$\frac{\partial T}{\partial z} = \pm c_1\sqrt{\frac{c_2}{\kappa_z}}\exp\left(\frac{c_2}{c_v}t \pm \sqrt{\frac{c_2}{\kappa_z}}z\right) \tag{6}$$

$C_1$ and $C_2$ are constants.

Equations 4–6 are derived under the assumption that both $C_v$ and $\kappa_z$ are constants. However, in reality, $C_v$ and $\kappa_z$ are not constants. Therefore, the relationship function needs to be confirmed using numerical experiments or data analysis.

Subsequently, using ERA5L reanalysis data, SMM was calculated based on the correlation coefficients between SM and subsequent SM or ST. The correlation between SM and the subsequent SM or ST expresses the projection of SM onto the subsequent SM or ST, and to some extent implies the effect of SM on subsequent SM or ST, that is, the response of the subsequent SM or ST to the antecedent SM anomalies. SM anomalies persist in two ways, the first being the response of subsequent SM to the SM anomalies (Persis_SM_SM), and the second being the response of subsequent ST to the SM anomalies (Persis_SM_ST). The STM was also calculated using the same approach. Persis_SM_SM represents the lag time when the correlation coefficient between the SM of a given soil layer and subsequent SM of a calculated soil layer drops below the 95% confidence level, and the calculated soil layer was obtained using a natural logarithmic function. This natural logarithmic function was obtained by fitting the relationships between lag time and the soil depth, at which the correlation coefficient between SM and subsequent SM is the largest (Figure 1). Take the calculation of the persistence of SM anomalies of the first soil layer in subsequent SM as an example. At different lag time $t_i$ ($i = 0,1,2,3,\cdots\cdots$), the soil layer $Z_i$ where the maximum of the correlation coefficients between $SM_{0,1}$ and subsequent SM in the four soil layers ($SM_{i,1}$; $SM_{i,2}$; $SM_{i,3}$; $SM_{i,4}$) is located was selected, and the first and second subscripts correspond to the lag time and soil layer, respectively. A linear regression of $Z_i$ is performed with the natural logarithm of $t_i$ as the independent variable, and regression value is $\hat{Z}_i$ .

$$\hat{Z}_i = a\ln(t_i) + b \tag{7}$$

$$\text{Persis\_SM\_SM} = F(\text{Corr}(SM_{1,1}, SM_{i,\hat{Z}_i}), i = 0,1,2\cdots\cdots) \tag{8}$$

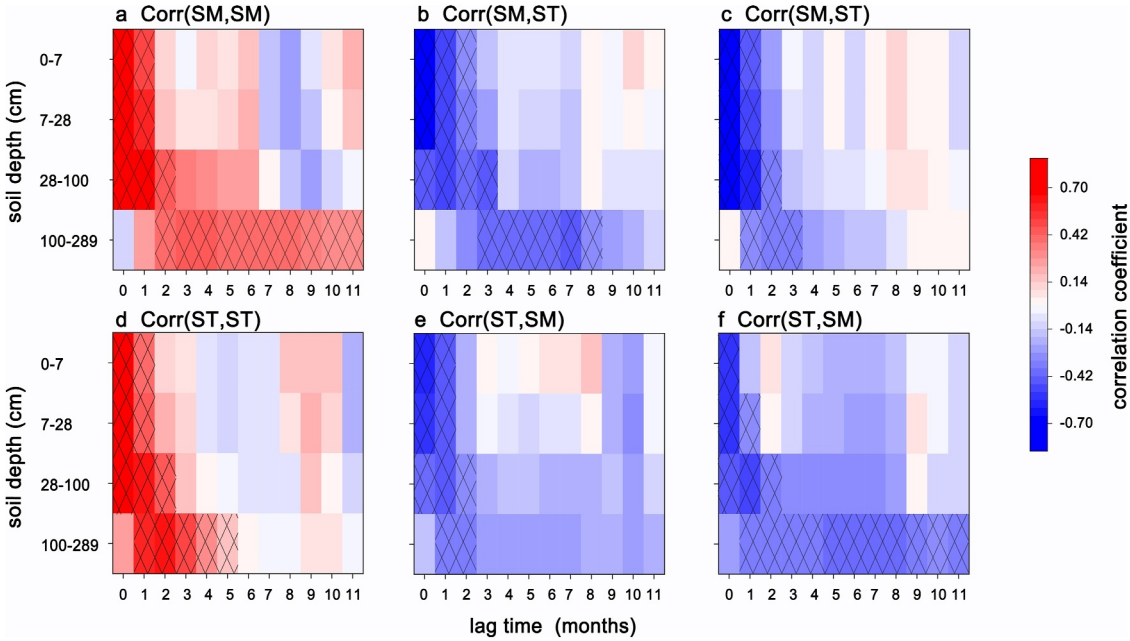


**Figure 2.** The correlation coefficients between the SM in the first soil layer and subsequent ST (a) or SM in the four soil layers (b, c) in July using ERA5L data. The correlation coefficients between the ST in the first soil layer and subsequent ST (d) or SM (e, f). (a–f) correspond to the spatial grid points (75.0°E, 31.5°N), (109.0°E, 42.0°N), (71.5°E, 33.0°N), (128.5°E, 40.5°N), (127.0°E, 51.0°N) and (85.0°E, 51.0°N), respectively. The rectangles with correlation coefficients passing the 95% confidence level are marked with slashes.

$a$ and $b$ are regression parameters. The function $F(\mathrm{Corr}(SM_{1,1}, SM_{i,\hat{Z}_i}), i = 0, 1, 2\cdots\cdots)$ is used to get the time when $\mathrm{Corr}(SM_{1,1}, SM_{i,\hat{Z}_i})$ drops below the 95% confidence level. $\mathrm{Corr}(SM_{1,1}, SM_{i,\hat{Z}_i})$ is the correlation coefficient between $SM_{1,1}$ and $SM_{i,\hat{Z}_i}$. Persis_SM_SM is the persistence time of SM anomaly signals in subsequent SM. $\mathrm{Corr}(SM_{1,1}, SM_{i,\hat{Z}_i})$ is the correlation coefficient between $SM_{1,1}$ and $SM_{i,\hat{Z}_i}$.

The same method was used in the calculations of Persis_SM_ST, Persis_ST_ST and Persis_ST_SM. The traditional method uses multi-year SM data from one soil layer to calculate SMM in this soil layer with a statistical approach, and it is based on the Euler perspective of a fixed soil layer, and the method in this study is based on the Lagrangian perspective of anomaly signals propagation in subsequent ST and SM. Within the Eulerian perspective, the memory of an anomaly is calculated from the e-folding time of its lagged autocorrelation (Amenu et al., 2005; Hu & Feng, 2004; Li et al., 2020; Wu & Dickinson, 2004; Yang & Zhang, 2016) in climate system. And this method assumes that the time series of variables is a first-order Markov process, and the probability of a given event occurring depends only on the state of the previous event in the sequence in a first-order Markov process. However, neither SM nor ST satisfies this assumption on month scale in China (Figure S1 in Supporting Information S1). According to the Eulerian perspective, if the anomaly signals at a given time (ASG) from other layers propagates to a certain layer after a period of time and there are weak correlations between the ASG at different soil layers, the other layers' ASG that propagates to this layer can neither be captured by the memory calculated in this layer nor by the memory calculated in other layers using these methods, but this ASG propagated to this layer is still the persistence of the ASG (Figure 2 and Figure S2 in Supporting Information S1). The performance of the Eulerian and Lagrangian perspectives in calculating memory was compared in Section 4.

Moreover, rainfall (Rainfall), evapotranspiration (Evap), radiation flux, sensible flux (SH) and other factors exert important influences on the spatial distributions of SM and ST. SMM and STM are mainly determined by the temporal variations of SM and ST, respectively. The temporal variations of SM are affected by rainfall and evapotranspiration (Equations 9 and 10). Meanwhile, the temporal dynamics of ST are modulated by radiation, water, sensible and latent fluxes (Equations 11 and 12). Based on Equations 9–12, the impact of Rainfall, Evap, SH, radiation flux and other factors on the spatial distributions of SMM and STM were analyzed.

$$\left(\frac{\partial SM}{\partial t}\right)_{\text{surface}} = -q_{\text{infil}} + \left(\text{Rain} - \text{Evap}_{\text{surface}}\right) \tag{9}$$

$$\frac{\partial SM}{\partial t} = -\frac{\partial q}{\partial z} - q_{\text{transpi}} \tag{10}$$

$$-\left(\frac{\partial \kappa(ST)}{\partial z}\right)_{\text{surface}} = S\text{net} - T\text{net} - SH - LE \tag{11}$$

$$\frac{\partial C_v(ST)}{\partial t} = \frac{\partial \kappa(ST)}{\partial z^2} \tag{12}$$

$\kappa$ is soil thermal conductivity. $z$ is soil depth. $C_v$ is volumetric soil heat capacity. $q_{\text{infil}}$ is water infiltration. $q$ is soil water flux. $q_{\text{transpi}}$ is transpiration loss by root. The subscript surface denotes the surface soil.

Furthermore, the spatial similarities of the STM across 4 soil depths and 12 months were analyzed using Pearson correlation coefficients, and the same analysis was done to SMM. The relationships between STM/SMM and precipitation, evaporation, radiation flux, heat flux, soil freezing and snow cover were investigated. Moreover, the temporal variations of STM and SMM were obtained by calculating 32 sliding STM and SMM with an 11-year window during 1980–2021. Empirical orthogonal function (EOF) analysis was applied to decompose SMM and STM variations across 4 soil depths and 12 months, identifying their dominant spatiotemporal patterns over China. SMM and STM are influenced by land surface variables, which are modulated by large-scale atmospheric or oceanic patterns at decadal time scale, such as AMO (the Atlantic Multidecadal Oscillation), DMI (the Dipole Mode Index), NAO (the North Atlantic Oscillation), PDO (the Pacific Decadal Oscillation), Niño3.4, SOI (the Southern Oscillation index), IPO (the Interdecadal Pacific Oscillation). And the relationships between these impact factors and STM/SMM were also analyzed.

### 2.3. Model Description and Experimental Design

To characterize the persistence of SM and ST anomalies in soil, providing a reference framework for the calculation of the memories of SM and ST using observational or reanalysis data, the CLM4.5 (Oleson et al., 2013) was employed. The CLM 4.5 is the land component of the Community Earth System Model (CESM), and it has been widely used in scientific researches. In this study, it was used to investigate the response of SM and ST to the SM or ST anomalies in initial conditions. The response can be considered as the persistence of the initial SM or ST anomaly signals in the subsequent ST and SM, or the memories of the initial SM or ST anomalies in the subsequent ST and SM. The variations of subsequent SM or ST anomalies with lag time and soil depth were studied to understand the persistence characteristics of the anomaly signals caused by the initial SM or ST anomalies. Then, the persistence characteristics of anomaly signals can be functionally represented through regression models incorporating both lag time and soil depth parameters. Based on the function, SMM and STM were calculated using reanalysis data. Three set of numerical experiments include one control experiment (CTL) and four sensitivity experiments were performed in Table 1, and four sensitivity experiments were carried out with wet (WET), hot (HOT), dry (DRY) and cold (COLD) anomalies in initial conditions, respectively. In the WET and DRY experiments, the initial SM conditions were obtained by doubling and halving the observed values, respectively. For the HOT and COLD experiments, the initial ST conditions were obtained by adding and subtracting 5°C from observations, respectively. As shown in Table 1, the anomalies of ST and SM were added for the shallow, middle and deep soil layers, respectively. The model integration begins on June 1st, so the anomalies were imposed in June 1st. The atmospheric forcing variables referred to the observation data at Tongyu site (122°52′E, 44°25′N), covering the period from 1 June 2024 to 31 December 2024. The land cover is degraded grassland. In Table 1, shallow, middle and deep soil correspond to 0–0.289, 0.289–1.38 and 1.38–3.80 m, respectively.

Moreover, the Weather Research and Forecasting (WRF) model 4.3 was used to analyze the memories of ST and SM anomalies in January and July. The simulation domain, centered at (35°N, 100°E), covers 80 grid points (west-east) × 50 grid points (south-north) with a 100 km horizontal grid spacing, using NCEP-FNL data for initial and boundary conditions. The Noah-MP land surface scheme was used in these simulations. To better evaluate the

**Table 1**
*Design of the Numerical Experiments for Different ST or SM Anomalies at Different Soil Depths in the Initial Conditions*

| | | Initial ST | Initial SM |
|---|---|---|---|
| Shallow soil | Control | Observed | Observed |
| | Cold anomaly | Observed | Observed −5°C |
| | Hot anomaly | Observed | Observed +5°C |
| | Wet anomaly | Observed × 2.0 | Observed |
| | Dry anomaly | Observed × 0.5 | Observed |
| Middle soil | Control | Observed | Observed |
| | Cold anomaly | Observed | Observed −5°C |
| | Hot anomaly | Observed | Observed +5°C |
| | Wet anomaly | Observed × 2.0 | Observed |
| | Dry anomaly | Observed × 0.5 | Observed |
| Deep soil | Control | Observed | Observed |
| | Cold anomaly | Observed | Observed −5°C |
| | Hot anomaly | Observed | Observed +5°C |
| | Wet anomaly | Observed × 2.0 | Observed |
| | Dry anomaly | Observed × 0.5 | Observed |

*Note.* "Observed" in the table is based on the observation at TongYu site in 2004.

simulation performance of WRF model using observational data, the simulation period was selected as 2023 to 2024, a time frame relatively close to the present.

Two control experiments (CTL-WRF-JAN, CTL-WRF-JUL) were performed starting from January 1 to 31 December 2023 and from 1 July 2023 to 30 June 2024, respectively. Four sensitivity experiments (JAN-ST, JAN-SM, JUL-ST, JUL-SM) were conducted, starting from January 2, January 2, July 2 and July 2, respectively. The atmospheric and soil conditions simulated by control experiments were used as the initial conditions of four sensitivity experiments after adding ST anomalies. The added ST anomalies were referenced to the standard deviation of the ERA5L ST and SM in January and July from 1979 to 2023. The memories of ST anomalies is defined as the simulation duration until the difference between ST simulated by the sensitivity experiment and ST simulated by the control experiment changes sign throughout the whole soil column, and the memories of SM anomalies were calculated in the same approach.

Precipitation significantly influences SM, and a very high correlation exists between T2m and ST. Therefore, the performance of the WRF model in simulating T2m and precipitation can, to some extent, reflect its capability in simulating SM and shallow ST. The monthly mean T2m and precipitation were used to evaluate the corresponding WRF simulations.

## 3. The Persistence Characteristics of SM and ST Anomaly Signals in Soil

The correlation between ST and subsequent ST indicates the projection of the ST onto the subsequent ST. Using the ERA5L data, Pearson correlation coefficients between the ST of the first soil layer for 12 months from January to December and the subsequent ST/SM in different soil layers were calculated, and then averaged over all spatial grids (70°E–135°E, 15°N–55°N) and over 12 months. Similar calculations were also performed for the ST in the other soil layers. Figure 3 shows the spatially (across China) and temporally (12 months of a year) averaged correlation coefficients between current SM or ST in the first soil layer and subsequent SM and ST across the four soil layers. It can be seen that the variations of ST and SM anomaly signals over time and with soil depth. ST anomalies can affect subsequent ST and SM, and persist over time through subsequent ST or SM anomalies (Figure 3). The same characteristics are present for SM anomalies (Figure 3). The above characteristics are critically important for quantifying the memories of SM or ST anomalies.

To understand the characteristics of the persistence of SM and ST anomaly signals in soil, several numerical experiments were carried out using CLM4.5. The initial SM anomalies can lead to the anomalies of subsequent SM and ST, while the ST anomalies similarly influence subsequent SM and ST anomalies (Figure 4). Therefore, the analysis on the persistence of either SM or ST anomalies in soil needs to consider the response of both SM and ST to initial SM or ST anomalies. Numerical simulations reveal that initial thermal anomalies (cold/hot) produce SM anomalies penetrating deeper soil layers over time, whereas initial hydrological anomalies (wet/dry) show no significant depth progression (Figures 4a and 4c). The soil depths of ST anomalies generally increase over simulation time, except when initiated by wet or shallow/mid-layer dry initial anomalies (Figures 4d and 4f). The different temporal variations of the soil depths where soil anomalies are located, caused by the initial wet anomalies and the initial shallow and middle dry anomalies, may stem from the limitations in the atmospheric forcing data used for the simulation. Moreover, the SM anomaly intensities caused by the initial cold and hot anomalies are much weaker than those caused by the initial wet and dry anomalies. The SM anomaly intensities caused by the initial wet and dry anomalies weaken over the simulation time (Figures 4g and 4i). The ST anomaly intensities caused by the initial cold and hot anomalies also weaken over the simulation time (Figures 4j and 4l). Figure 5 shows the variations of soil depth and intensity of the subsequent anomaly signals caused by the ST and SM of the first soil layer over simulation time. It can be seen that the anomaly signal of the first layer has the

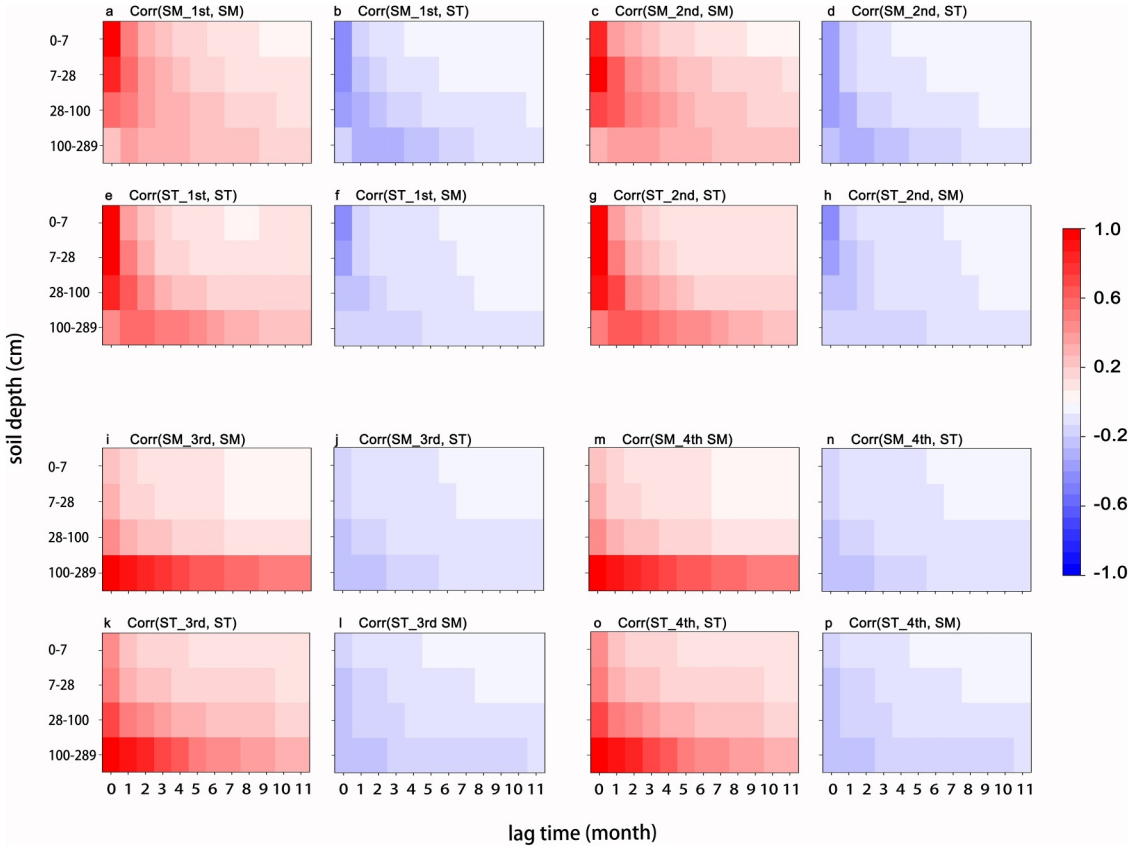


**Figure 3.** The spatially (across China) and temporally (12-month) averaged correlation coefficients between the ST/SM of the first (a, b, e, f), second (c, d, g, h), third (i–l) or fourth (m–p) soil layer and subsequent ST/SM of the four soil layers. _1st, _2nd, _3rd and _4th represent SM or ST in the first, second, third and fourth soil layers, respectively. Corr(SM_1st, SM) is the correlation coefficients between SM in the first soil layer and subsequent SM in the four soil layers.

characteristics of weakening and propagating downwards over time. Overall, in most cases, the soil depths of SM and ST anomalies induced by initial anomalies increase over simulation time, while their intensities become weak.

Using the data fitting method, it's found that both the intensities of anomaly signals and the soil depths of maximum signal intensity, induced by initial anomalies, follow natural logarithmic functions of simulation time. As shown in Table 2, in most cases, natural logarithmic functions can represent the characteristics of the anomaly signals caused by the initial anomalies over the simulation time. Therefore, it can be concluded that the memories of SM or ST anomalies in the subsequent SM and ST can be expressed by natural logarithmic functions, both in terms of the intensities and locations of subsequent anomaly signals.

## 4. The Comparison Between the Eulerian and Lagrangian Perspectives

To evaluate the performance of Euler and Lagrangian perspectives in calculating the memories, several cases were analyzed. As shown in Figure 2, SM and ST anomaly signals propagate downward over time, and the persistence time of the anomaly signals in subsequent ST and SM is the memory time. According to the Lagrangian perspective in this study, the STM of the first soil layer is 5 months, and the ST anomaly signals of the first soil layer propagate downward over time (Figure 2d). However, using traditional Euler method, the STM of the first soil layer is 1 month, and the statistically significant anomaly signals (as indicated by correlations, Figure 2) in the other soil layers can't be captured in the calculation of STM in Figure 2d. Several similar cases are also shown in Figures 2a–2c, 2e and 2f. Moreover, in Figure S1 of Supporting Information S1, using traditional Euler method, the STM of the first, second, third and fourth soil layers are 1, 1, 1 and 0 months, respectively, and the ST anomaly signals can only persist for up to 1 month. However, according to the method in this study, the STM of the first, second, third and fourth soil layers are 7, 7, 7 and 0 months, respectively, and the ST anomaly

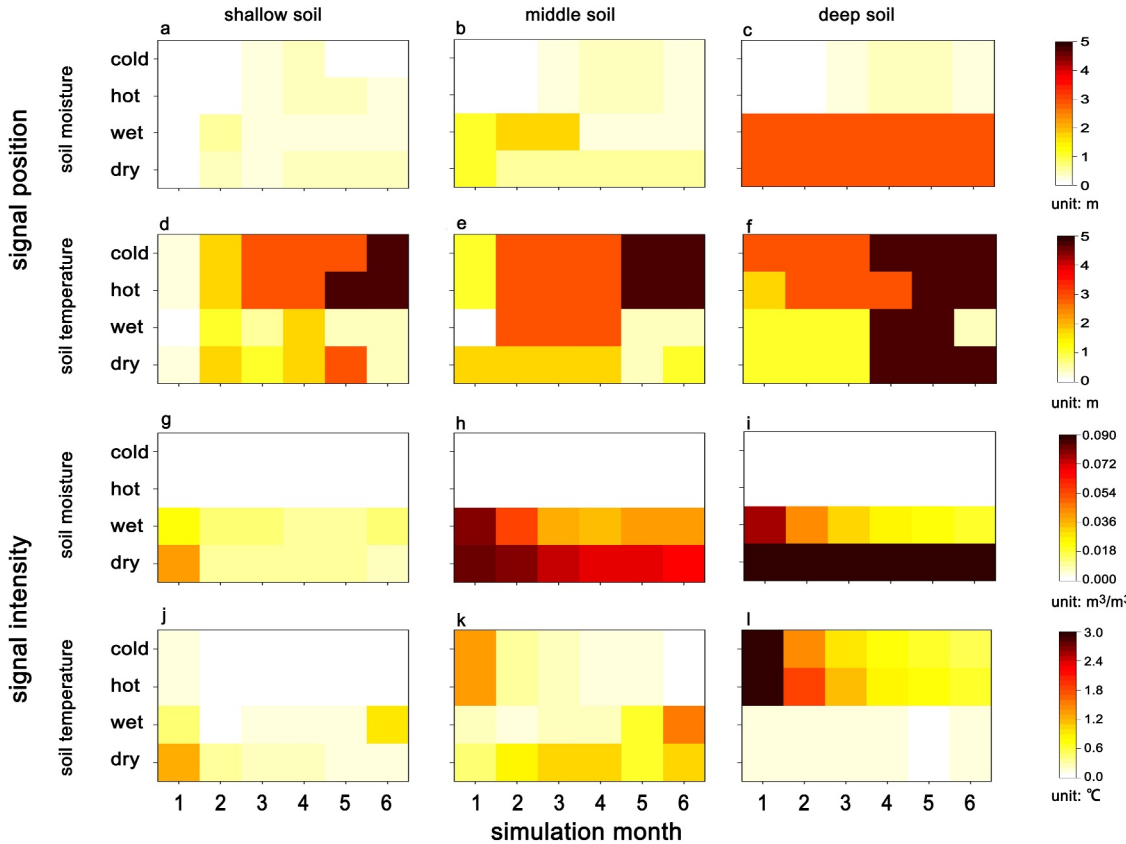


**Figure 4.** The response of SM (first and third rows) and ST (second and fourth rows) to the initial cold, hot, wet and dry anomalies in shallow (first column), middle (second column) and deep soil (third column) in the numerical experiments. The first and second rows correspond to the soil depths at which the strongest signals caused by the initial anomalies. The third and fourth rows correspond to the intensity of the anomaly signals caused by the initial anomalies.

signals can persist for up to 7 months (Figure S2 in Supporting Information S1). Additionally, referring to preliminary numerical experiments, the method used in this study is closer to real physical processes (Figure 5).

## 5. Evaluation of the ERA5L ST and SM With Observational Data

Because only the first-layer ST observations have fewer missing values (8.2%), it is inappropriate to use the observed ST to calculate the STM. In this study, reanalysis data is used to calculate the STM after evaluating their ability of representing the STM from observations. The significant lag correlation between ST and subsequent ST is an important feature of STM. The evaluation criterion is the time when the lag correlation coefficient between the ST of the first soil layer and the subsequent ST of the first soil layer drops below 99% confidence level (TimeLagCor_1st). First, the ERA5L spatial grid points closest to the 1117 sites were selected. Second, the sites and spatial grids with a given TimeLagCor_1st are assigned a value of 1, and the rest sites and spatial grids are assigned a value of 0. The selected ERA5L spatial grids were also processed in the same way. Finally, the correlation coefficients between the spatial distributions of ERA5L grid values and observation site values were calculated. These correlation coefficients represent the ability of the ERA5L ST to reproduce the TimeLagCor_1st calculated using the observed ST. Figure 6 shows that the ERA5L reanalysis can reproduce the spatial distributions of the TimeLagCor_1st calculated using observations when the TimeLagCor_1st is 0 and 1 month. As the memory length increases, the spatial consistency of the TimeLagCor_1st obtained from the ERA5L data and the ones from observations is significantly weakened (Figure 6). In a word, ERA5L data can represent the spatial distributions of the sites with short TimeLagCor_1st obtained from observations.

The SM observation spans 1991 to 2010 with numerous missing values, and the proportion of missing values is 73.4%. Therefore, it is not appropriate to use the method of evaluating STM (Figure 6). Referring to the method of Li et al. (2020), the correlation coefficients between the observed SM (0.1–0.2 m averages) and the ERA5L SM in

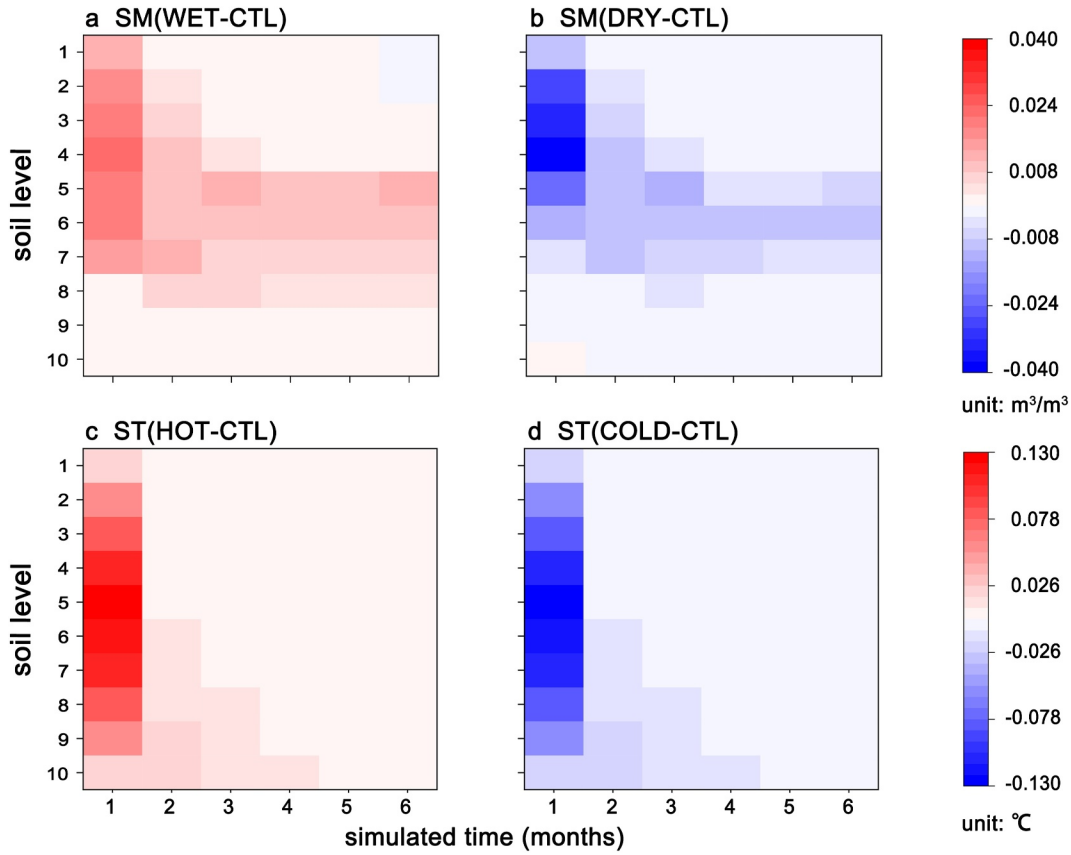


**Figure 5.** The SM anomalies and ST anomalies caused by the wet (a), dry (b), hot (c) and cold (d) anomalies of shallow soil in initial conditions using land surface model CLM4.5.

**Table 2**

*The Correlation Coefficients Between the Time Variations of the Intensities of Anomaly Signals Caused by the Initial SM or ST Anomalies and the Corresponding Fitted Natural Logarithmic Curves, and the Correlation Coefficients Between the Time Variations of the Soil Depths of Anomaly Signals Caused by the Initial SM or ST Anomalies and the Corresponding Fitted Logarithmic Curves*

| | | Depth-SM | Anomaly-SM | Depth-ST | Anomaly-ST |
|---|---|---|---|---|---|
| Shallow soil | Cold anomaly | 0.48 | 0.87 | 0.94** | 0.94** |
| | Hot anomaly | 0.83* | 0.81* | 0.97** | 0.97** |
| | Wet anomaly | 0.11 | 0.83* | 0.25 | 0.90** |
| | Dry anomaly | 0.76* | 0.85** | 0.39 | 0.26 |
| Middle soil | Cold anomaly | 0.83* | 0.79* | 0.92** | 0.92** |
| | Hot anomaly | 0.83* | 0.78* | 0.92** | 0.90** |
| | Wet anomaly | 0.61 | 0.90** | 0.02 | 0.63 |
| | Dry anomaly | 0.81* | 0.94** | 0.62 | 0.65 |
| Deep soil | Cold anomaly | 0.83* | 0.39 | 0.83* | 0.96** |
| | Hot anomaly | 0.83* | 0.33 | 0.88** | 0.97** |
| | Wet anomaly | 0.99** | 0.97** | 0.37 | 0.18 |
| | Dry anomaly | 0.99** | 0.94** | 0.83* | 0.45 |

*Note.* * and ** denote significance at $p < 0.05$ and $p < 0.01$, respectively.

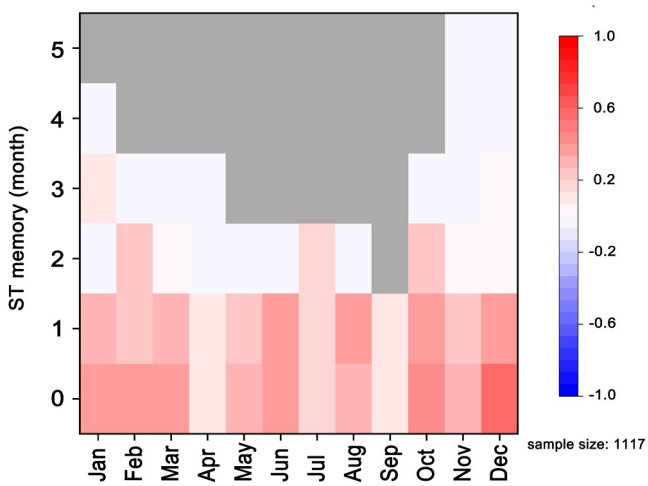


**Figure 6.** The correlation coefficients between the spatial distributions of ERA5 spatial grids and the spatial distribution of 1117 sites with same TimeLagCor_1st. TimeLagCor_1st is the time at which the correlation coefficient between the ST of the first soil layer and the subsequent ST of the first soil layer drops below 99% confidence level. The sites and spatial grids with a given TimeLagCor_1st are assigned a value of 1, and the rest sites and spatial grids are assigned a value of 0.

the second soil layer are used to quantify their consistency (Figure 7). The SM observations are from January 1991 to December 2020, with a large number of missing values. Figure 7a shows that the ERA5L SM data can well reproduce the temporal variations of the observed SM.

## 6. The Characteristics of SMM and STM in China

### 6.1. The Spatial Distributions of the STM and SMM in China

Figure 8 show the memories of SM and ST anomalies stored in subsequent ST and SM. It should be noted that Jan and Jul correspond to the time of the initial SM and ST anomalies, while 1st and 4th level correspond to the locations of the initial SM and SM anomalies in Figure 8. Pesis_SM_SM is significantly longer than Persis_SM_ST in January and July (Figure 8). Except the first soil layer in July, Persis_ST_ST is also longer than Persis_ST_SM. The spatial distributions of Persis_SM_SM of the first and fourth soil layers are similar in both January and July. Persis_SM_SM of the fourth soil layer is greater than 10 months in Northeast China (38°N–53°N, 115°E–135°E), North China (32°N–42°N, 104°E–125°E), Northwest China (35°N–50°N, 73°E–108°E) and the northwest part of the Qinghai-Tibet Plateau (25°N–35°N, 67°E–104°E). These sub-regions are illustrated in Figure S3 of Supporting Information S1. Persis_SM_SM of the first soil layer is greater than 10 months in Northeast China, North China and northwest part of the Qinghai-Tibet Plateau (Figures 8a, 8e, 8i and 8m). In the southern part of China (<30°N), Persis_SM_SM is about 1 month and 3 months in July and January, respectively, and significantly lower than in other regions. Moreover, Persis_SM_SM of the first soil layer is about 1 month in January in the northwest part of the China. In January, Persis_SM_ST of the first soil layer ranges from one to 11 months in North China and the Qinghai-Tibet Plateau, and 0 months in other regions (Figure 8b). In January, Persis_SM_ST of the fourth soil layer is mainly in the range of 3–11 months in eastern part of China, and mainly around 0 months in other regions (Figure 8f). In July, Persis_SM_ST is mainly from 0 to 2 months (Figure 8n).

The spatial distributions of Persis_ST_ST of the first and fourth soil layers are similar in January, and Persis_ST_ST is about 11 months in Northeast China and the southeast part of the Qinghai-Tibet Plateau. In Northwest China, Persis_ST_ST of the first and fourth soil layers in January is about 1 month and 11 months, respectively. In the other regions, Persis_ST_ST is mainly from 3 to 6 months in January (Figures 8c and 8g). In July, the Persis_ST_ST of the first soil layer is mainly from 5 to 11 months in North China, Southwest China and the southeastern parts of Tibet Plateau, and the values range from 0 to 4 months in the other regions (Figure 8k). In

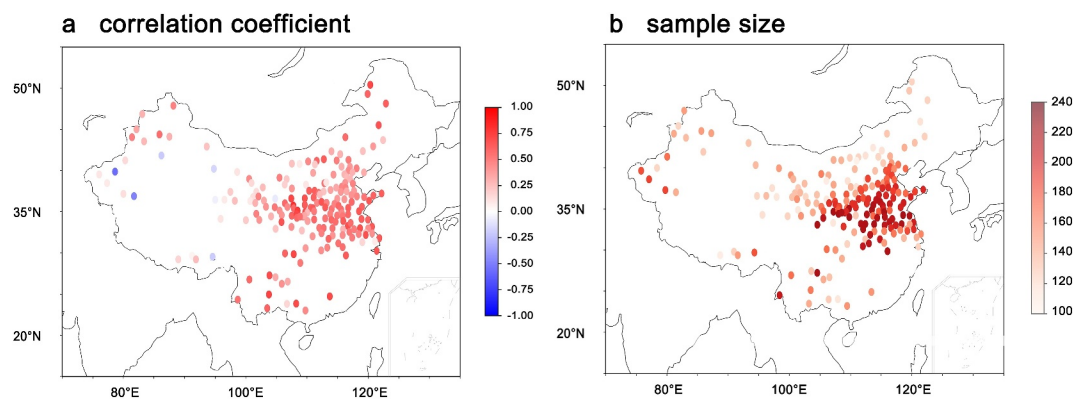


**Figure 7.** The correlation coefficients between the observed SM averaged at 0.1 and 0.2 m depth and the ERA5 SM in the second soil layer. The maximum sample size is 240 (20 years multiply 12 months). Due to missing values, only the correlation coefficients with sample size greater than 100 are shown. (a, b) correspond to correlation coefficients and sample sizes, respectively.

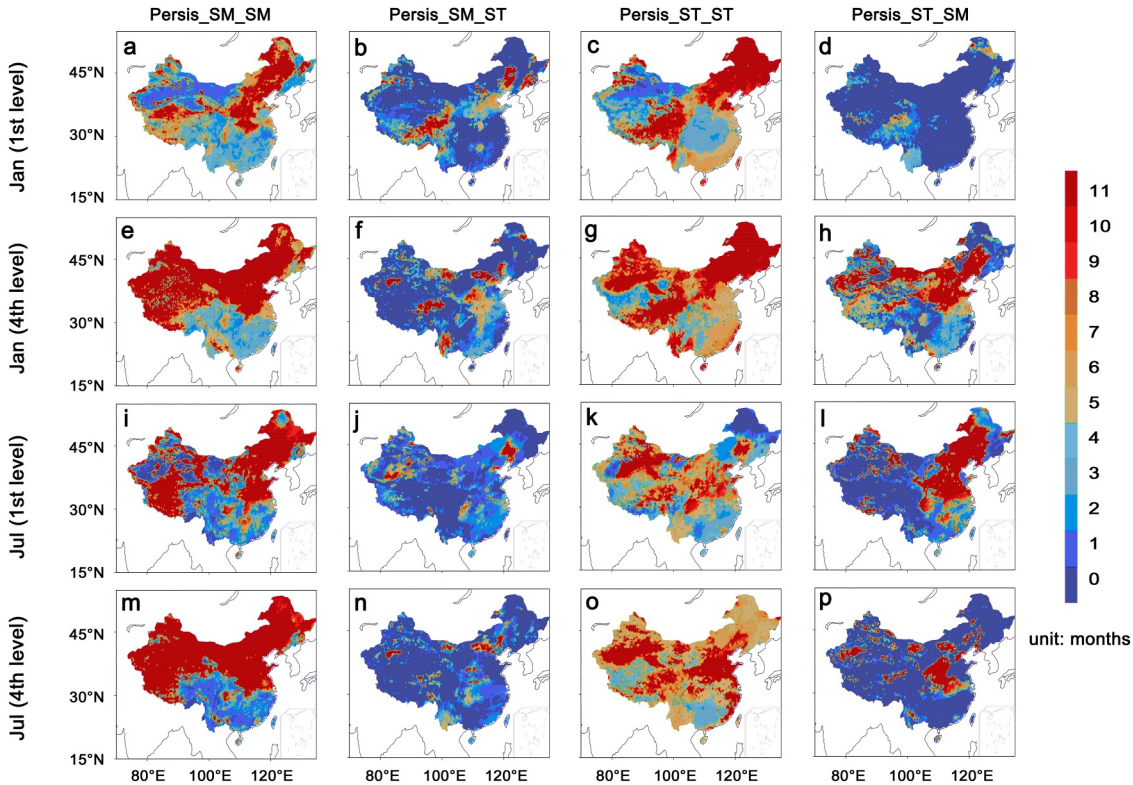


**Figure 8.** The memories of SM and ST in subsequent SM or ST. The first, second, third and fourth columns correspond to the memories of SM in subsequent SM (Persis_SM_SM), and the memories of SM in subsequent ST (Persis_SM_ST), the memories of ST anomalies in subsequent ST (Persis_ST_ST) and the memories of ST anomalies in subsequent SM (Persis_ST_SM), respectively. The first and second rows correspond to the memories of SM or ST in the first and fourth soil layers in January, respectively, while the third and fourth rows correspond to the memories of SM or ST in the first and fourth soil layers in July, respectively.

July, the Persis_ST_ST of the fourth soil layer is mainly from 5 to 11 months in North China, Northeast China, Southwest China and the southeastern parts of Tibet Plateau, and the values range from 3 to 4 months in the other regions (Figure 8o). The Persis_ST_SM of the first soil layer in January is 0 months in most parts of China, except Yunnan and the eastern part of the Qinghai-Tibet Plateau, where the memory ranges from 2 to 6 months (Figure 8d). The Persis_ST_SM of the fourth layer in January ranges from 5 to 11 months in Northwest China, North China, and the southern part of Northeast China. Persis_ST_SM in January ranges from 0 to 4 months in the southern part of China and about 5 months in the Qinghai-Tibet Plateau (Figure 8h). In the first layer in July, Persis_ST_SM is mainly 11 months in Huanghuai, North China and the eastern part of Northeast China, while the memory is about 0 months in the rest of China (Figure 8l). In the fourth layer, Persis_ST_SM in July is mainly 11 months in the region (30°N–40°N, 105°E–115°E), and the memory is mainly 0 months in the rest of China (Figure 8).

Overall, the memory increases with soil depth. The memories of SM in subsequent SM are longer than the ones of SM in subsequent ST, while the memories of ST in subsequent ST are longer than the ones of ST in subsequent SM. Moreover, the memory is long in North China, Northeast China, Qinghai-Tibet Plateau and Northwest China. The memory is very short in the southern part of China. Persis_SM_ST and Persis_ST_SM are 0 months in many parts of China.

Morevoer, the spatial distributions of 12-month average STM and SMM were analyzed. The maximum value of Persis_SM_SM averaged over 12 months for the four soil layers and Persis_SM_ST averaged over 12 months for the four soil layers is named Persis_SM. Persis_ST is similarly defined. As shown in Figure 9, long Persis_SM has a larger spatial extent than long Persis_ST in the northern part of China, and Persis_SM is shorter than Persis_ST in the southern part of China. Persis_SM is longer in North China, Northeast China, Northwest China and the western part of Qinghai-Tibet Plateau than in the rest of China, even up to 11 months. Persis_SM is short in the southern part of China, about 2–4 months (Figure 9a). Persis_ST is longer in North China, the southwestern

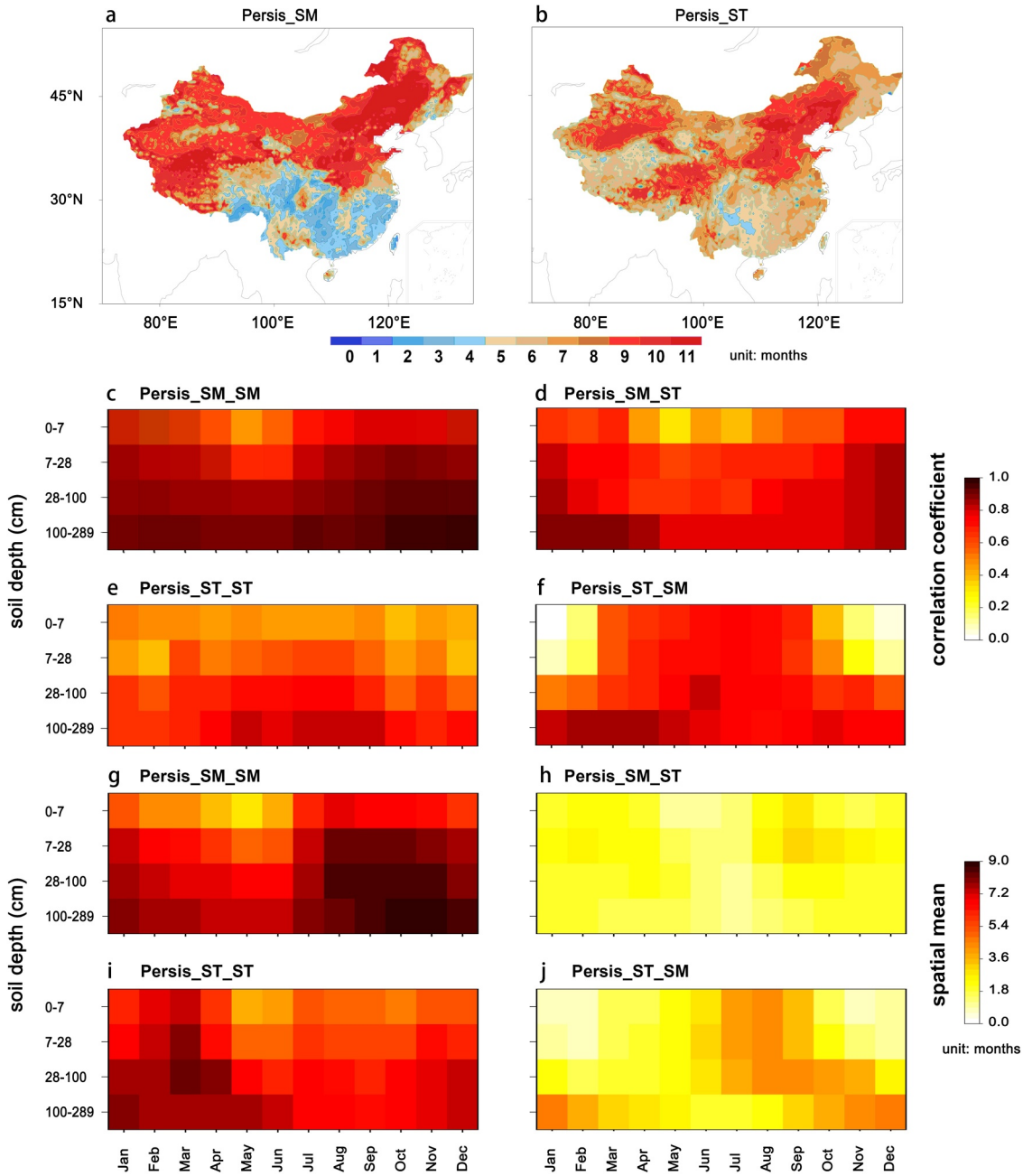


**Figure 9.** The spatial distribution of Persis_SM (a) and Persis_ST (b). The maximum value of Persis_SM_SM averaged over 12 months for the four soil layers and Persis_SM_ST averaged over 12 months for the four soil layers is named Persis_SM. Persis_ST is similarly defined. (c–j) represent the similarity of the spatial distributions of Persis_ST/Persis_SM across months and inter-monthly variation of spatial means. (c–f) show the correlation coefficients between the spatial distributions of the 12-month average Persis_ST/Persis_SM and the spatial distributions of the monthly Persis_ST/Persis_SM. (c–f) correspond to Persis_SM_SM, Persis_SM_ST, Persis_ST_ST and Persis_ST_SM, respectively. (g–j) are the Persis_ST and Persis_SM averaged over all spatial grid points in China from January to December in the four soil layers. (g–j) correspond to Persis_SM_SM, Persis_SM_ST, Persis_ST_ST and Persis_ST_SM, respectively. The sample size is 12,197.

part of Northeast China, Northwest China and the southeastern part of Qinghai-Tibet Plateau than in the rest of China, even up to 11 months. However, Persis_ST is short in the southern part of China, about 4–7 months (Figure 9b). On the whole, Persis_SM and Persis_ST are longer in North China, Northeast China, Northwest China and Qinghai-Tibet Plateau than in the rest of China. The STM in 12 months have high spatial similarity with the 12-month average STM, and so does SMM (Figures 9c–9j). The similarity is higher in deep soil layers, and higher in the winter half-year for Persis_SM_SM and Persis_SM_ST, and higher in the summer half-year for

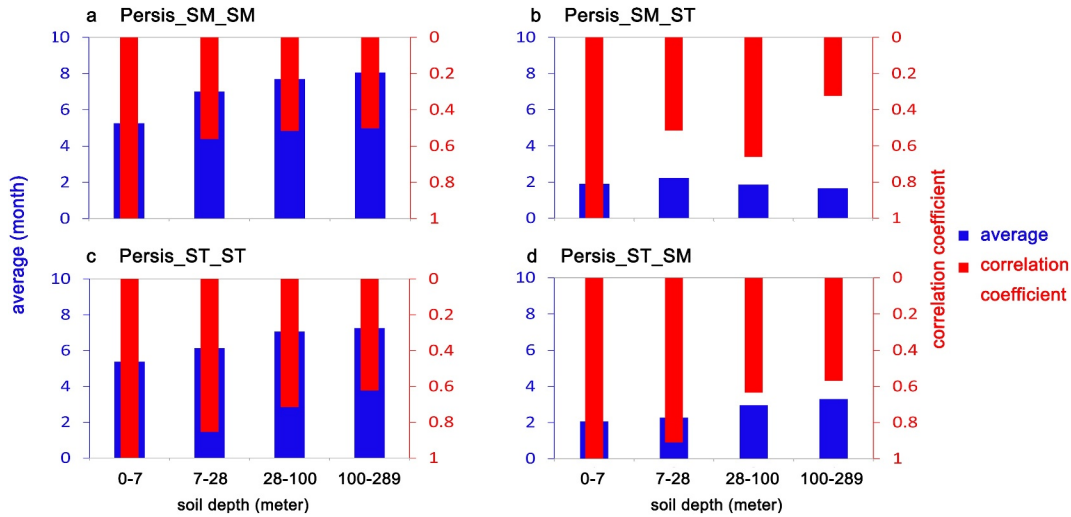


**Figure 10.** The 12-month mean STM/SMM averaged over all spatial grid points in China, and the spatial correlation coefficients between 12-month mean STM/SMM in the first soil layer and the 12-month mean STM/SMM in the first, second, third and fourth soil layers. (a–d) correspond to Persis_SM_SM, Persis_SM_ST, Persis_ST_ST and Persis_ST_SM, respectively.

Persis_ST_SM (Figures 9c–9j). There are significant monthly variations for Persis_ST_SM (Figure 10), which is also shown in Figure 8. Figures 9c and 9f show that Persis_SM_SM and Persis_ST_SM are longer in the second half of the year, and they have similar spatial pattern. More precipitation starting from July leads to positive SM anomalies and negative ST anomalies, and these anomalies caused by precipitation will persist in the form of SM anomalies. Figure 9i shows that Persis_ST_ST is longer from January to April, which is attributed to less precipitation that makes the persistence of ST anomalies less disturbed from January to April. Figures 9h and 9i show that Persis_SM_ST and Persis_ST_ST have similar spatial pattern. Moreover, Persis_SM_ST and Persis_ST_SM are much smaller than Persis_SM_SM and Persis_ST_ST, which is also shown in Figure 8.

Figure 10 shows that the SMM of the second, third and fourth soil layers is highly spatial similar to the SMM of the first soil layer, as is STM. The spatial correlation coefficients between Persis_SM_SM of the first layer and those of the second, third, and fourth layers are 0.56, 0.52, and 0.50, respectively. The spatial correlation coefficients between Persis_SM_ST of the first layer and those of the second, third, and fourth layers are 0.52, 0.66, and 0.32, respectively. The spatial correlation coefficients between Persis_ST_ST of the first layer and those of the second, third, and fourth layers are 0.85, 0.72, and 0.62, respectively. The spatial correlation coefficients between Persis_ST_SM in the first layer and those in the second, third, and fourth layers are 0.91, 0.63, and 0.57, respectively. In addition, the spatial similarities of Persis_SM_ST at different depths are smaller. Moreover, the 12-month mean Persis_SM_SM across China are 5.3, 7.0, 7.7 and 8.1 months in the four soil layers, respectively, while 12-month mean Persis_SM_ST across China are 1.9, 2.2, 1.9 and 1.7 months in the four soil layers, respectively. The 12-month mean Persis_ST_ST across China are 5.4, 6.1, 7.1 and 7.3 months in the four layers, respectively, while 12-month mean Persis_ST_SM across China are 2.1, 2.3, 3.0 and 3.3 months in the four layers, respectively (Figure 10).

### 6.2. The Memories of SM and ST Anomalies Stored in Shallow Soil and Related Physics Processes

Shallow SM and ST directly modulate land-atmosphere interactions through water, heat and radiation fluxes (Oleson et al., 2013); therefore, the influence of SM and ST on subsequent shallow SM and ST is very important for climate prediction.

Using SMM and STM data, the maximum lead time of antecedent SM and ST that can affect current SM or ST of the first layer can be obtained, and named as Persis_SM_SM_1st, Persis_SM_ST_1st, Persis_ST_ST_1st and Persis_ST_SM_1st. As shown in Figure 11, the lead time roughly ranges from 0 to 5 months across China, with 1 month persistence being most common, except for Persis_SM_SM_1st in winter/summer/autumn and Persis_ST_SM_1st in autumn/winter. Persis_SM_SM_1st is about from 6 to

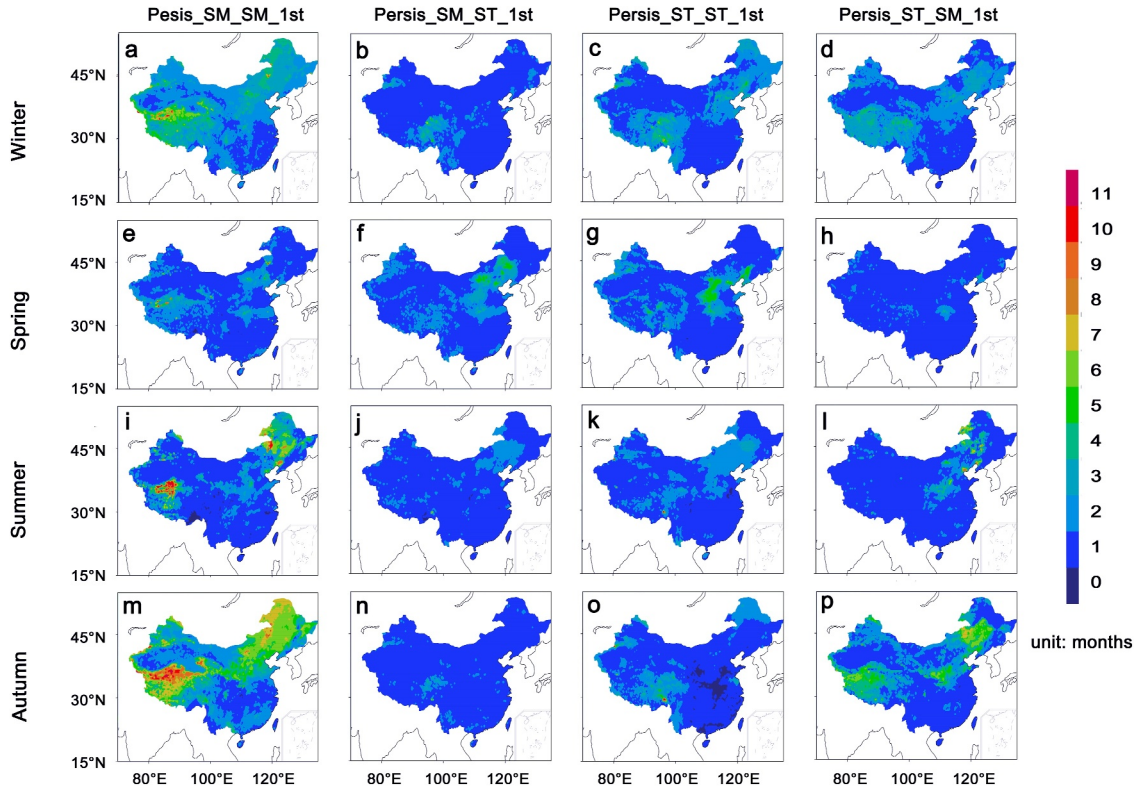


**Figure 11.** The persistence time of antecedent SM and ST anomalies in subsequent SM or ST of the first soil layer. The first, second, third and fourth columns correspond to the persistence time of SM anomalies in subsequent SM of the first soil layer (Persis_SM_SM_1st), and the persistence time of SM anomalies in subsequent ST of the first soil layer (Persis_SM_ST_1st), the persistence time of ST anomalies in subsequent ST of the first soil layer (Persis_ST_ST_1st) and the persistence time of ST anomalies in subsequent SM of the first soil layer (Persis_ST_SM_1st), respectively. The first and second rows correspond to the persistence time of SM or ST anomalies in winter and spring, respectively, while the third and fourth rows correspond to the persistence time of SM or ST anomalies in summer and autumn, respectively.

10 months in the northern part of the Qinghai-Tibet Plateau and the western part of Northeast China in winter, summer and autumn (Figures 11a, 11i and 11m). Moreover, Persis_ST_SM_1st is about from 4 to 6 months in autumn and is about from 2 to 3 months in winter in the northern part of the Qinghai-Tibet Plateau and the southern part of Northeast China in autumn (Figure 11p). Overall, lead time is longer in Northeast China, North China and Qinghai-Tibet Plateau. The maximum lead time of antecedent SM and ST affecting ST or SM of the first soil layer are at least 1 month in most parts of China.

Figures 12a–12e show that the SM and ST anomalies of the first soil layer can persist in the first soil layer and propagate downward in soil over time. The persistence time of antecedent SM or ST anomalies in the SM or ST of the first soil layer is denoted as PST. The processes in which antecedent ST or SM of the second, third and fourth soil layers affects ST or SM of the first soil layer are similar to the processes by which antecedent ST or SM of the first soil layer affects ST or SM of the first soil layer (Figure 12). However, the locations of the antecedent strongest signals are different. Moreover, the similar patterns shown in Figure 12 are attributed to the high correlations between the SM/ST of different soil depths. In addition, the anomalies can persist for longer time in deeper soil.

### 6.3. The SMM and STM Derived From WRF Simulations

The simulated T2m and Rainfall can well reproduce the spatial patterns of the observed ones in January and July 2023 (Figure S4 in Supporting Information S1). However, the simulated T2m is lower than the observed in most regions of China in January. In most areas of the Tibet Plateau and northeastern China, the simulated T2m shows a cold bias of 4–10°C relative to observations. In July, the simulated T2m shows negative biases of 0–10°C in the southern parts of China, and positive biases of 0–6°C in the northern parts of China compared to observations. The

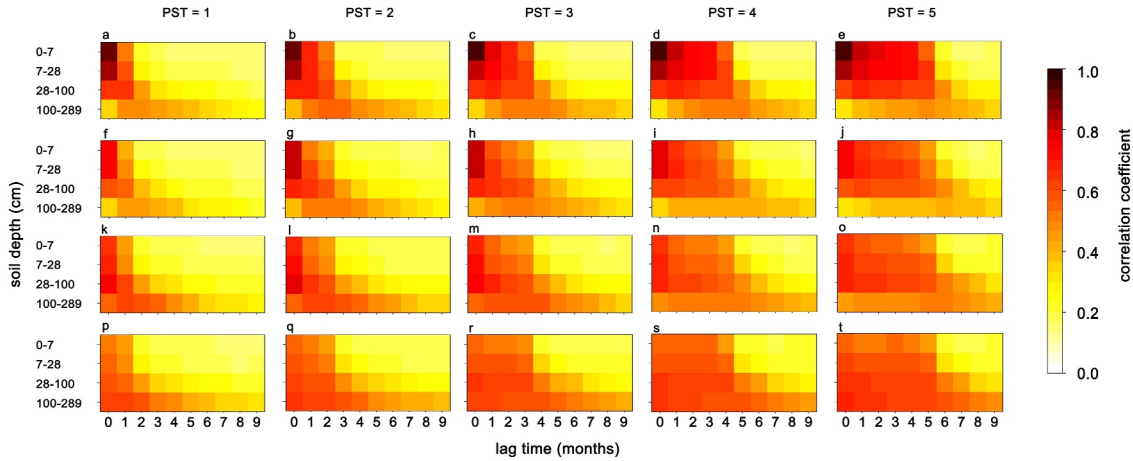


**Figure 12.** The processes by which SM and ST anomalies propagate in soil, affecting subsequent ST or SM in the first soil layer. These processes are described by the spatial average of the correlation coefficients. PST denotes the persistence time of SM or ST anomalies in subsequent SM or ST in the first soil layer. The first, second, third, fourth and fifth columns correspond to the PST of 1, 2, 3, 4 and 5 months, respectively. The antecedent ST or SM anomalies, affecting the subsequent ST or SM of the first soil layer after the PST time, are located in the first (first row), second (second row), third (third row) and fourth (fourth row) soil layers.

simulated rainfall reproduces the observed spatial patterns in January, except in the southeastern parts of China. Compared to observations, the simulation significantly underestimates precipitation by up to about 50 mm in some regions of the southeastern parts of China. In July, the simulated rainfall can reproduce the observed spatial pattern. However, the simulation shows systematic biases by overestimating rainfall in high-rainfall regions and underestimating in low-rainfall regions. For instance, the simulated rainfall is up to 200 mm higher in southwestern parts of China and up to 200 mm lower in the southeastern parts of China.

As shown in Figure 13, the simulated SMM exhibits a spatial distribution similar to that of the SMM derived from ERA5L in January (Figure 13a). However, the simulated SMM is significantly shorter than those derived from ERA5L reanalysis data (Figure 13a). In July, both the ERA5L and the simulated SM exhibit longer memories in

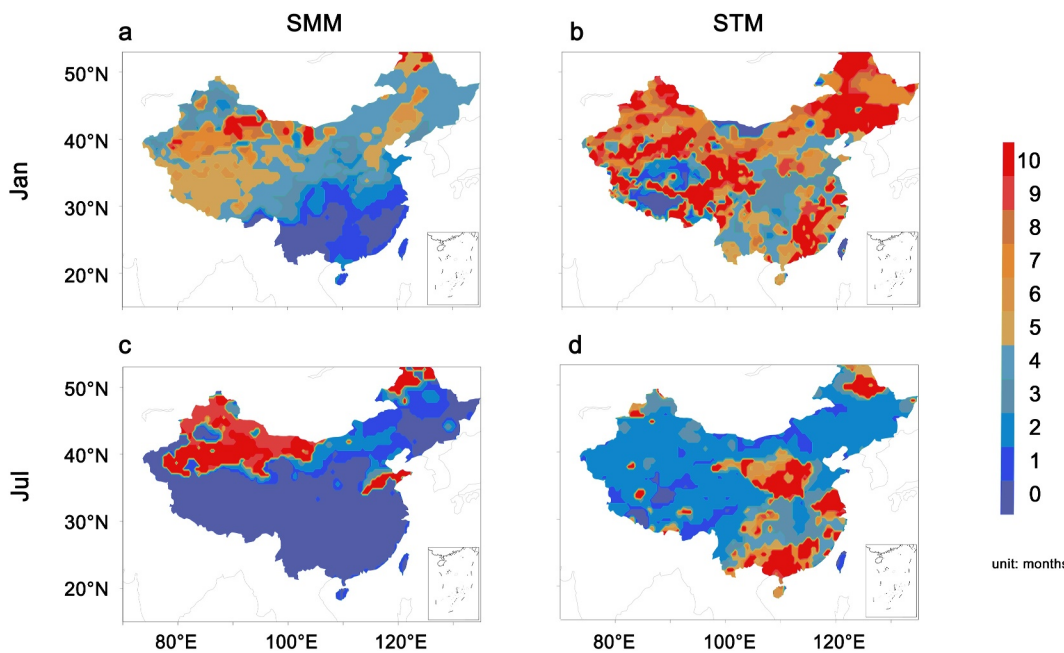


**Figure 13.** WRF-simulated memories of ST and SM anomalies of the whole soil column. (a, c) inllustrate the memories of SM anomalies on January 1 and 1 July 2023, respectively. (b, d) correspond to the memories of ST anomalies on January 1 and 1 July 2023, respectively.

the northern parts of China relative to the southern parts of China (Figure 13c). But in Tibet Plateau, most of North China and northeastern China, the simulated SMM is about 0 months, while the ERA5L SMM is about 11 months (Figure 13c). In January, the spatial pattern of the simulated STM shows high consistency with those derived from ERA5L data. Compared to the ERA5L STM, the simulated STM is about 10 months shorter in the southern parts of Tibet Plateau and about 3 months longer in the southeastern parts of China, respectively (Figure 13b). In July, both the ERA5L and simulated STM are shorter in Tibet Plateau, northeastern China and South China. The simulated STM is about 7 months shorter in northwestern China and the southeastern parts of Tibet Plateau, while the simulated STM is about 6 months longer in regions south of 25°N (Figure 13d).

In summary, the simulated STM and SMM exhibit generally consistent spatial patterns with the ERA5L ones, though their values are systematically lower than the latter in some regions. The discrepancies between the simulated memories and those from ERA5L may be attributed to the performance of the model (Figure S4 in Supporting Information S1) as well as the short simulation period. The memories derived from the data during 1979–2023 should differ from the memories in 2023.

### 6.4. The Factors Associated to the Spatial Distributions of SMM and STM

Rainfall, evapotranspiration (Evap), radiation flux, sensible flux (SH) and other factors exert important influences on the spatial distributions of SMM and STM. SMM and STM are mainly determined by the temporal variations of SM and ST, respectively. The temporal variations of SM are affected by rainfall and evapotranspiration (Equations 9 and 10). Meanwhile, the temporal dynamics of ST are modulated by radiation, water, sensible and latent fluxes (Equations 11 and 12).

As shown in Figure 14, the linear relationship between SMM and Evap as well as rainfall differs entirely, with the boundary being 600 mm of rainfall and 400 mm of Evap. The boundary corresponds to the semi-arid and semi-humid regions. To the north of the boundary, SMM increases as rainfall and Evap rise; to the south, it decreases as rainfall and Evap increase. The variations of SM are controlled by energy and water in the south and the north of the boundary, respectively. The long-term memory of SM anomalies requires both an appropriate amount of soil water storage and relatively little energy exchange.

Figure 14 show that the spatial distributions of Persis_ST are significantly correlated with the spatial distributions of net solar radiation (Snet), net thermal radiation (Tnet), latent heat flux (LE) and rainfall. Moreover, the linear relationships between STM and these impact factors exhibit distinct characteristics in Inner Mongolia, northwestern China, and the Tibetan Plateau compared to other regions. The geographical boundary between these two types of regions is defined by critical thresholds of rainfall (500 mm), Tnet (80 $W/m^2$) and LE (35 $W/m^2$) (Figure 14). To the north of the boundary lies the arid and semi-arid region, while to the south is an area controlled by monsoons (Figure S5a in Supporting Information S1). STM exhibits the characteristics of decreasing as LE and rainfall increase, and increasing as Tnet increases (Figure 14).

Moreover, the spatial distribution of snow cover is not significantly linearly related to the spatial distributions of Persis_SM and Persis_ST. Overall, more precipitation trends to diminish ST anomalies persistence, while appropriate rainfall is conductive to the persistence of SM anomalies.

## 7. The Temporal Variations of SMM and STM in China

### 7.1. The Temporal Variations of SMM and STM

There are strong decadal and monthly variations in SMM and STM (Figure 15). Based on 11-year moving correlation coefficients, SMM and STM are obtained at each spatial grid at four soil depths in 12 months. Then, SMM and STM are decomposed into different spatial patterns and the variations of the spatial patterns with soil depth, month and year by the EOF method. The explained variances of the first EOF modes are 51.4%, 18.1%, 44.1% and 26.7% for Persis_SM_SM, Persis_SM_ST, Persis_ST_ST and Persis_ST_SM, respectively. Figure 15 shows the decadal and monthly variations corresponding to the first leading EOF modes, and the explained variances of the first leading EOF modes of Persis_SM_SM and Persis_ST_ST are obviously bigger than those of Persis_SM_ST and Persis_ST_SM. There are obvious decadal signals in Persis_SM_SM and Persis_SM_ST, while the annual signals are more obvious in Persis_ST_ST and Persis_ST_SM. Referring to Figure 15, the STM at different soil depths have similar monthly and decadal variations, and so does the SMM. The similar decadal variations are shown in Persis_SM_SM and Persis_SM_ST (Figures 15e and 15f). Moreover, Persis_ST_ST and

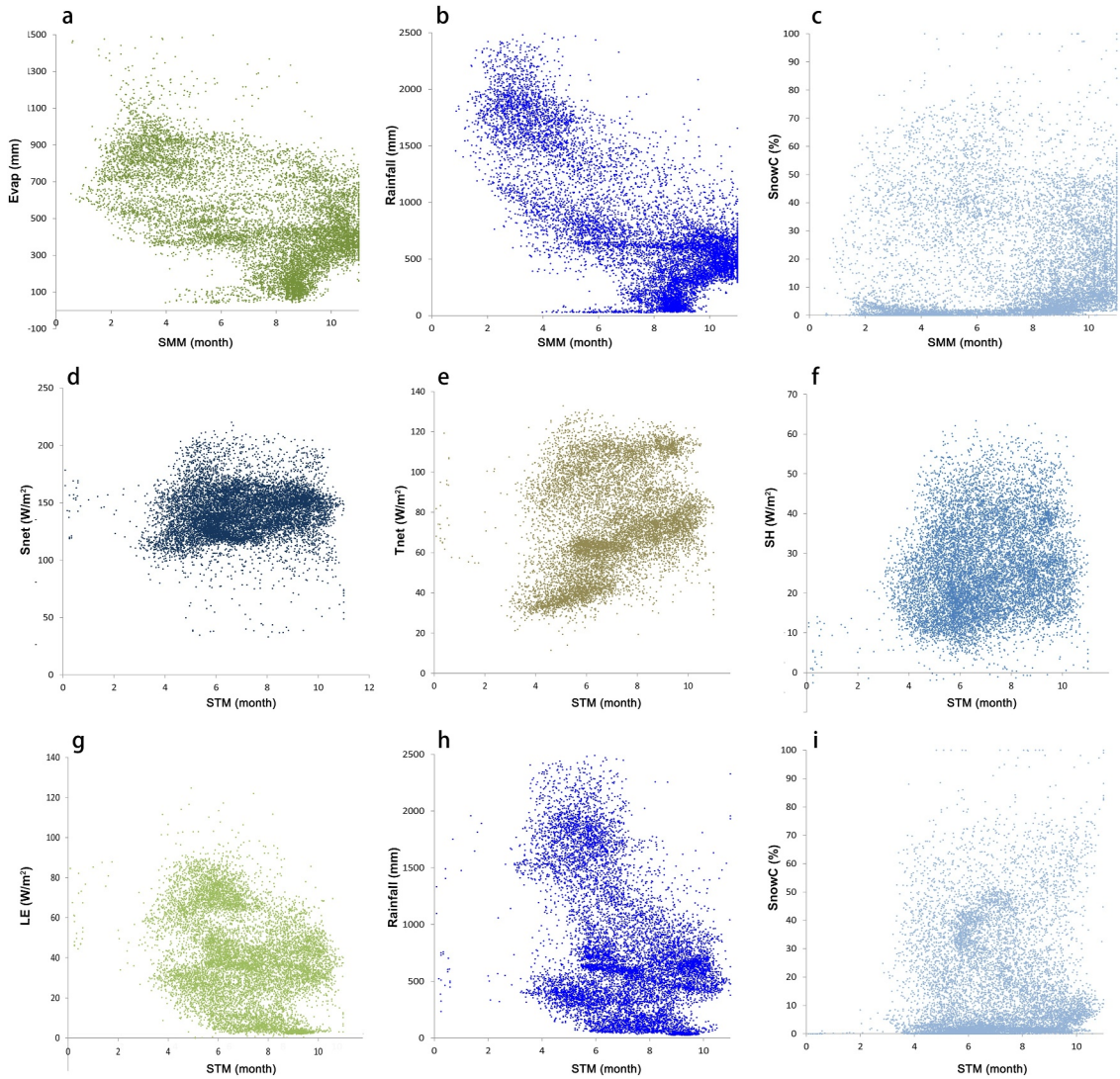


**Figure 14.** The comparison of the Persis_SM/Persis_ST with rainfall (Rainfall), Evap, snow cover (SnowC), Snet, Tnet, LE and SH. Rainfall, Evap, SnowC, Snet, Tnet, LE and SH are averaged over all months from 1979 to 2022. Persis_SM and Persis_ST are the average value of the four soil layers over 12 months.

Persis_SM_ST have similar monthly variations, while Persis_SM_SM and Persis_ST_SM also have similar monthly variations (Figures 15l–15o). The anomalies stored in subsequent SM can persist longer in the non-flood and cold season (Figures 15l and 15o), and the anomalies stored in subsequent ST can persist longer in non-flood season (Figures 15m and 15n).

Corresponding to the monthly and decadal variations of the first EOF mode in Figure 15, the spatial patterns of the first EOF modes are shown in Figures 15a–15d. The spatial patterns are very similar to the spatial patterns of the SMM and STM in Figure 8. For Persis_SM_SM, high values are located in the northwest of Qinghai-Tibet Plateau, North China, and Northeast China (Figure 15a). For Persis_SM_ST, high values are mainly located in the eastern part of Qinghai-Tibet Plateau, the western part of Northwest China, North China and the southern part of Northeast China (Figure 15b). For Persis_ST_ST, high values are located in the eastern part of Qinghai-Tibet Plateau, the Northeast China (Figure 15c). For Persis_ST_SM, the high values are mainly located in the eastern part of Qinghai-Tibet Plateau, North China and Northeast China (Figure 15d). The higher values correspond to longer memory and greater monthly and annual variations of STM or SMM in Figure 15, according to the formula of the EOF method.

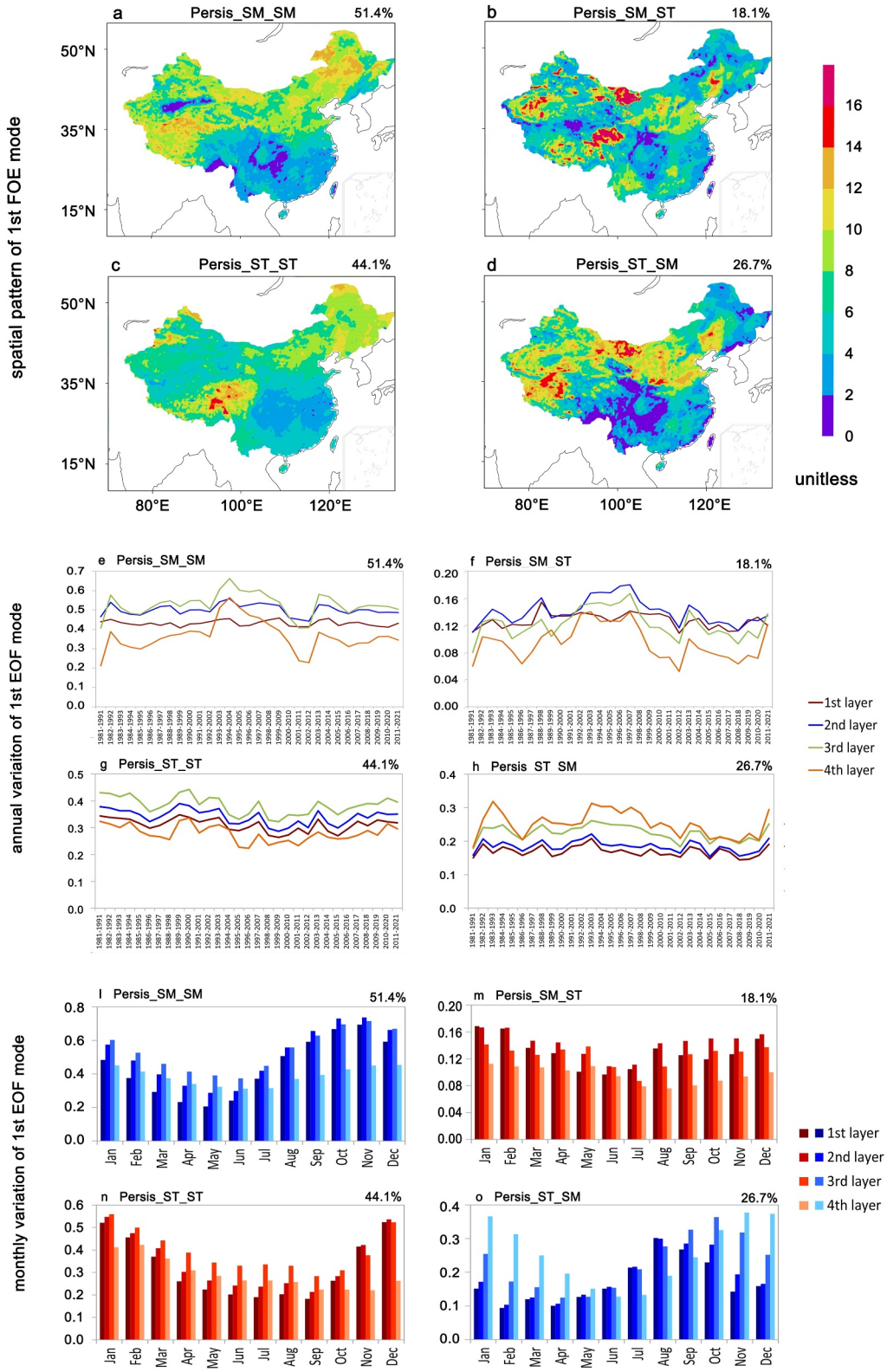


**Figure 15.** The spatial patterns (a–d), decadal variations (e–h), monthly variations (l–o) of the first leading EOF modes of STM and SMM. (a, e, l) correspond to Persis_SM_SM (b, f, m) correspond to Persis_SM_ST. (c, g, n) correspond to Persis_ST_ST. (d, h, o) correspond to Persis_ST_SM. The number in each panel denotes the explained variance of the first EOF mode.

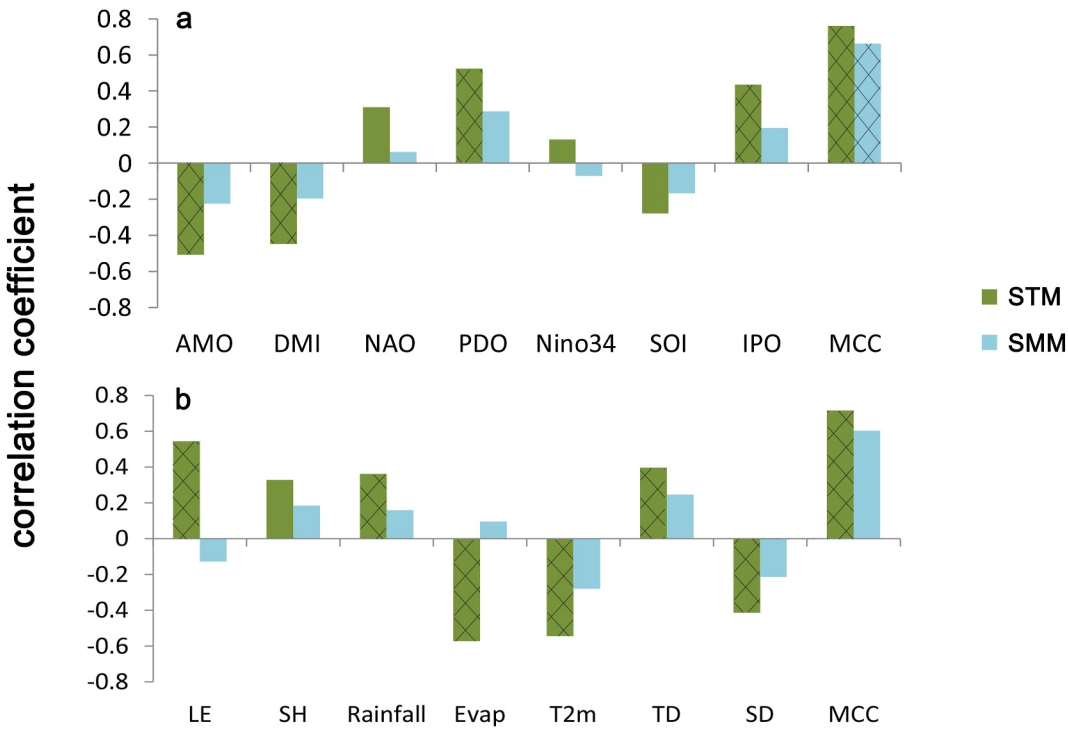


**Figure 16.** The correlation coefficients between the temporal variations of some impact factors and the decadal variations of the first leading EOF modes of STM and SMM. MCC denotes multiple correlation coefficient, which was calculated using 7 climate indices and 7 land surface variables in panels (a, b). All impact factors were processed using an 11-year moving average, and then averaged over 12 months and across all spatial grids in China. The 7 land surface variables include LE, SH, Rainfall, Evap, T2m, TD and SD. The rectangles with statistically significant correlations ($p < 0.05$) are cross-hatched.

### 7.2. The Factors Affecting the Temporal Variations of SMM and STM

The decadal variations of rainfall, Evap, radiation and heat fluxes show significant linear correlations with the memory lengths of ST anomalies, and the multiple correlation coefficient (MCC) between STM and these land surface variables is bigger than 0.7 (Figures 16b). However, the linear relationships between these land surface variables and SMM are not statistically significant, which may suggest the existence of complex nonlinear relationships between them (Figures 14 and 16b). These land surface variables are modulated by atmospheric circulation which is affected by large-scale atmospheric or oceanic patterns at annual and decadal time scale. The correlation coefficients between the climate indices and the temporal variations of the first EOF modes of STM/SMM in Figure 15a are calculated. As shown in Figure 15a, Persis_ST_ST has a closer relationship with the climate indices, and the MCC is 0.76 (Figure 15a). In addition, although SMM exhibits no significant linear relationships with these climate indices, the MCC between SMM and these climate indices reaches 0.66, showing statistical significance at the 95% confidence level, which may be associated with the nonlinear relationships between SMM and these land surface variables.

Nonlinear relationships characterize both the spatial distributions (Figure 14) and monthly variations (Figure 17) of SMM in relation to rainfall and Evap. Figure 18a shows that the persistence time of SM anomalies before the concentrated rainfall period is about 8 months, while that after the concentrated rainfall period is about 10 months. More Rainfall disrupts the persistence of SM anomalies. According to Equations 11 and 12, enhanced LE, SH, downward thermal radiation (TD) and downward solar radiation (SD) all shorten the persistence of ST anomalies (Figure 17b). Moreover, the freeze-thaw process also has an important influence on SMM. As shown in Figure 18, the variances of subsequent SM explained by current SM are significantly greater under frozen condition than those under unfrozen condition. And the difference can reach up to 50% (Figures 18a and 18f). The frozen soil enhances soil water storage capacity by reducing drainage and suppressing evaporation. However, the persistence of ST anomalies is not related to the freeze-thaw process. No significant differences in the persistence of ST anomalies are found between frozen and unfrozen soil (Figures 18c, 18d, 18h and 18i).

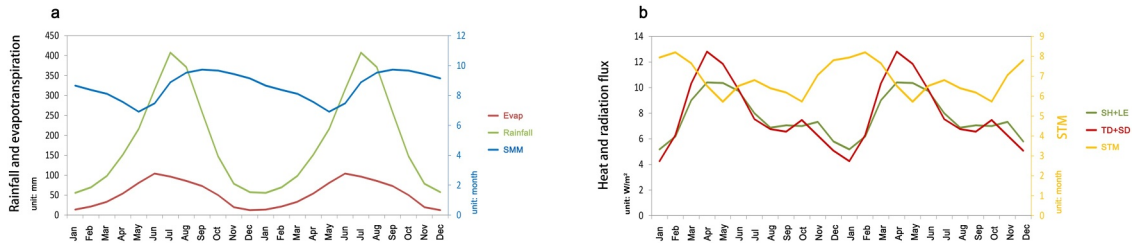


**Figure 17.** The monthly variations in STM, SMM, Rainfall, Evap, SH plus LE and TD plus SD averaged over 1979–2023 and cross spatial grids with values exceeding 9 in Figures 18a and 18c.

## 8. Conclusions and Discussions

The persistence of antecedent SM and ST anomalies establishes the connection among the antecedent SM and ST, subsequent SM and ST, and subsequent atmosphere. The ERA5 reanalysis data, CLM4.5 and WRF4.3 were used in this study. As a complement to the Eulerian approach, the Lagrangian approach was used in this study. The spatial patterns of lag autocorrelations of shallow ST derived from ERA5L show good agreement with the observation when lag time is not long. The ERA5L data can reproduce well the temporal variations of observed SM. The simulations by CLM4.5 show that the location to which the SM or ST anomaly signals propagate in soil over time is a natural logarithmic function of lag time, and the intensity of the anomaly signals caused by the initial SM or ST anomalies is also a natural logarithmic function of lag time. Moreover, the anomaly signals of ST can persist in form of the anomalies of subsequent SM, and vice versa. The results show that Persis_SM_SM and Persis_ST_ST are longer than Persis_SM_ST and Persis_ST_SM. Persis_SM_SM is approximately 9–11 months in North China, Northeast China, Northwest China and the northwest part of Qinghai-Tibet Plateau than in the rest of China The memory length is about from 1 to 4 months in the southern part of China. The spatial distributions of Persis_SM_ST vary greatly in different months, and it ranges between 0 and 2 months in most regions of China. For Persis_ST_ST, the high values are mainly in Northeast China, Northwest China, North China and the eastern part of Qinghai-Tibet Plateau, and the values range between 0 and 11 months across months and soil depths. Additionally, Persis_ST_SM of first and fourth soil layers is longer and extend to 11 months in January and July, respectively, in North China. The above conclusions are based on the analysis in January and July, and the spatial distributions of the memory lengths may be different for other months, although there are some similarities in the spatial distributions across different months. STM and SMM increase significantly with soil depth. Moreover, considering the importance of ST and SM anomalies of shallow soil in land-atmosphere interactions, the persistence of antecedent ST and SM anomalies in subsequent shallow soil was investigated. The results show that the memory time is about 1 month in most regions of China, and high values are mainly located in Qinghai-Tibet Plateau, Northeast China and North China, where the memory time can even reach 11 months. Moreover, the SMM and STM simulated by WRF exhibit generally consistent spatial patterns with the ERA5L ones, though their values are systematically lower than the ones derived from ERA5L in some regions. The discrepancies

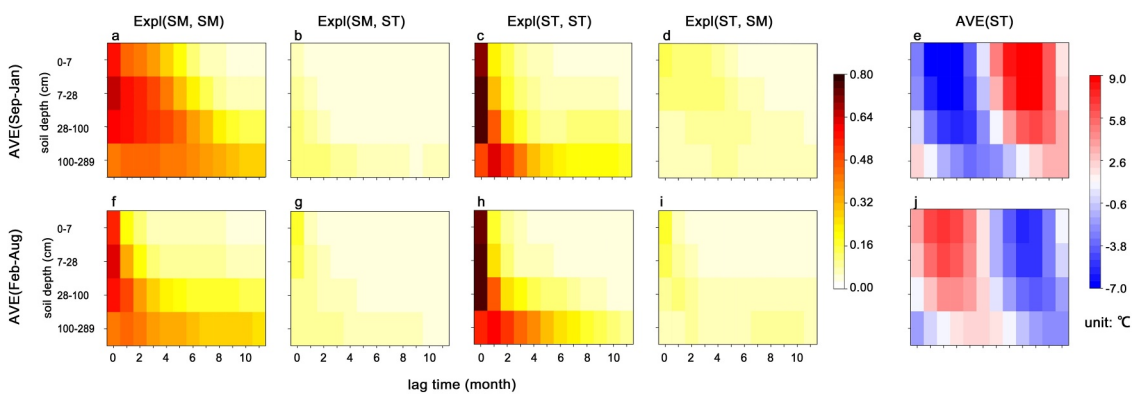


**Figure 18.** The monthly variations in STM, SMM, Rainfall, Evap, SH plus LE and TD plus SD averaged over 1979–2023 and cross spatial grids with seasonal freezing in Figures 18a and 18c.

between the simulated and ERA5L memories may be related to the WRF performance as well as the short simulation period.

The spatial patterns of SMM are closely related to those of rainfall and Evap, while the spatial patterns of STM exhibit strong correlations with those of Snet, Tnet, LE and rainfall. The relationships between SMM/STM and land surface variables exhibit distinct characteristics in arid and wet regions. Climate indices (e.g., AMO, NAO) modulate the decadal variations of STM through their impacts on land surface fluxes. Meanwhile, the linear relationship between SMM and climate indices is not statistically significant; instead, their relationship is nonlinear, regardless of regional differences or monthly variations. More Rainfall disrupts the persistence of SM anomalies, while enhanced LE, SH, TD and SD shorten the persistence of ST anomalies. Moreover, the SMM is significantly greater under frozen condition than that under unfrozen condition, and the difference can reach up to 50%, because the frozen soil enhances soil water storage capacity by reducing drainage and suppressing evaporation. The STM is not related to the freeze-thaw process. Additionally, the related physical processes of the atmospheric factors affecting SMM and STM were not studied in depth in this paper, and the processes may be space- and time-dependent, and need to be studied by a lot of numerical experiments. Some studies have confirmed that soil texture (Liu et al., 2020; Song et al., 2019), soil column depth (Liu et al., 2020) and freeze-thaw process (Li et al., 2021; Schaefer et al., 2007) play an important role in ST and SM memories.

In the reanalysis-based study, the primary focus was on assessing linear relationships among these variables. However, both the persistence of SM or ST anomalies and the influence of climate indices and land surface variables on the persistence include linear and nonlinear processes, although linear processes may be dominant. The exclusion of nonlinear processes in these analytical methods may introduce discrepancies between our findings and actual physical relationships. Nevertheless, the idea of this method has important reference significance for understanding the memories of the anomalies of various variables in the earth system. The STM and SMM derived from numerical simulation and statistical analysis can be compared with each other to reduce uncertainty in understanding the role of land surface variables in climate prediction. Furthermore, sparse observational coverage (particularly over the Tibetan Plateau, southern China, and northeastern China) limits the robust evaluation of ERA5L ST and SM data, introducing uncertainties in subsequent analyses. Quantitative comparisons reveal that ERA5L and observations are not entirely consistent, potentially affecting result reliability

## Conflict of Interest

The authors declare no conflicts of interest relevant to this study.

## Data Availability Statement

ERA5 reanalysis data is from the European Center for Medium-Range Weather Forecasts (ECMWF) (Hersbach et al., 2023a, 2023b). ERA5-Land reanalysis data are available at the Copernicus Climate Change Service Data Store (Muñoz Sabater, 2019). Regarding the site-observed soil temperature and soil moisture data, due to China's data policies, anyone can register an account on the website and then apply for downloads. The site data of soil temperature is from the China Meteorological Data Service Centre, which can be obtained from: http://www.nmic.cn/data/detail/dataCode/A.0012.0001.html. Soil moisture data is also from the China Meteorological Data Service Centre, which can be obtained from: https://data.cma.cn/site/subjectDetail/id/101.html. Daily precipitation and air temperature observation data at 2 m are from National Centers for Environmental Information (https://www.ncei.noaa.gov/maps/daily).

**Acknowledgments**
This work was supported by the National Natural Science Foundation of China (Grants 42130609, 41975081 and 41005047).

## References

Amenu, G. G., Kumar, P., & Liang, X. Z. (2005). Interannual variability of deep-layer hydrologic memory and mechanisms of its influence on surface energy fluxes. *Journal of Climate*, *18*(23), 5024–5045. https://doi.org/10.1175/JCLI3590.1

Benson, D. O., & Dirmeyer, P. A. (2023). The soil moisture–surface flux relationship as a factor for extreme heat predictability in subseasonal to seasonal forecasts. *Journal of Climate*, *36*(18), 6375–6392. https://doi.org/10.1175/JCLI-D-22-0447.1

Beven, K. J., & Kirkby, M. J. (1979). A physically based, variable contributing area model of basin hydrology/Un modèle à base physique de zone d'appel variable de l'hydrologie du bassin versant. *Hydrological Sciences Journal*, *24*(1), 43–69. https://doi.org/10.1080/02626667909491834

Delworth, T., & Manabe, S. (1988). The influence of potential evaporation on the variabilities of simulated soil wetness and climate. *Journal of Climate*, *1*(5), 523–547. https://doi.org/10.1175/1520-0442(1988)001<0523:TIOPEO>2.0.CO;2

Dong, X., Zhou, Y., Chen, H., Zhou, B., & Sun, S. (2022). Lag impacts of the anomalous July soil moisture over Southern China on the August rainfall over the Huang–Huai River Basin. *Climate Dynamics*, *58*(5–6), 1737–1754. https://doi.org/10.1007/s00382-021-05989-1

Entin, J. K., Robock, A., Vinnikov, K. Y., Hollinger, S. E., Liu, S., & Namkhai, A. (2000). Temporal and spatial scales of observed soil moisture variations in the extratropics. *Journal of Geophysical Research*, *105*(D9), 11865–11877. https://doi.org/10.1029/2000JD900051

Gao, C., Chen, H., Li, G., Ma, H., Li, X., Long, S., et al. (2019). Land–atmosphere interaction over the Indo-China Peninsula during spring and its effect on the following summer climate over the Yangtze River basin. *Climate Dynamics*, *53*(9–10), 6181–6198. https://doi.org/10.1007/s00382-019-04922-x

Gao, C., Li, G., Chen, H., & Yan, H. (2020). Interdecadal change in the effect of Spring soil moisture over the Indo-China peninsula on the following summer precipitation over the Yangtze River Basin. *Journal of Climate*, *33*(16), 7063–7082. https://doi.org/10.1175/JCLI-D-19-0754.1

Hersbach, H., Bell, B., Berrisford, P., Hirahara, S., Horányi, A., Muñoz-Sabater, J., et al. (2023a). ERA5 monthly averaged data on pressure levels from 1940 to present [Dataset]. *Copernicus Climate Change Service (C3S) Climate Data Store (CDS)*. https://doi.org/10.24381/cds.6860a573

Hersbach, H., Bell, B., Berrisford, P., Hirahara, S., Horányi, A., Muñoz-Sabater, J., et al. (2023b). ERA5 monthly averaged data on single levels from 1940 to present [Dataset]. *Copernicus Climate Change Service (C3S) Climate Data Store (CDS)*. https://doi.org/10.24381/cds.f17050d7

Hsu, H., Lo, M. H., Guillod, B. P., Miralles, D. G., & Kumar, S. (2017). Relation between precipitation location and antecedent/subsequent soil moisture spatial patterns. *Journal of Geophysical Research: Atmospheres*, *122*(12), 6319–6328. https://doi.org/10.1002/2016JD026042

Hu, Q., & Feng, S. (2004). A role of the soil enthalpy in land memory. *Journal of Climate*, *17*(18), 3633–3643. https://doi.org/10.1175/1520-0442(2004)017<3633:arotse>2.0.co;2

Jones, R. H. (1975). Estimating the variance of time averages. *Journal of Applied Meteorology*, *14*(2), 159–163. https://doi.org/10.1175/1520-0450(1975)014<0159:ETVOTA>2.0.CO;2

Koster, R. D., & Suarez, M. J. (2001). Soil moisture memory in climate models. *Journal of Hydrometeorology*, *2*(6), 558–570. https://doi.org/10.1175/1525-7541(2001)002<0558:SMMICM>2.0.CO;2

Kumar, S., Newman, M., Wang, Y., & Livneh, B. (2019). Potential reemergence of seasonal soil moisture anomalies in North America. *Journal of Climate*, *32*(10), 2707–2734. https://doi.org/10.1175/JCLI-D-18-0540.1

Li, M., Wu, P., Ma, Z., Lv, M., & Yang, Q. (2020). Changes in soil moisture persistence in China over the past 40 years under a warming climate. *Journal of Climate*, *33*(22), 9531–9550. https://doi.org/10.1175/JCLI-D-19-0900.1

Li, Q., Xue, Y., & Liu, Y. (2021). Impact of frozen soil processes on soil thermal characteristics at seasonal to decadal scales over the Tibetan Plateau and North China. *Hydrology and Earth System Sciences*, *25*(4), 2089–2107. https://doi.org/10.5194/hess-25-2089-2021

Lin, Z., Zuo, Z., Zhang, R., Xiao, D., You, Q., & Qiao, L. (2022). Persistence of soil enthalpy drives the winter and summer climate connection in the Tibetan Plateau. *Geophysical Research Letters*, *49*(12), e2022GL098503. https://doi.org/10.1029/2022GL098503

Liu, D., Wang, G., Mei, R., Yu, Z., & Yu, M. (2014). Impact of initial soil moisture anomalies on climate mean and extremes over Asia. *Journal of Geophysical Research: Atmospheres*, *119*(2), 529–545. https://doi.org/10.1002/2013JD020890

Liu, Y., & Avissar, R. (1999). A study of persistence in the land-atmosphere system using a general circulation model and observations. *Journal of Climate*, *12*(8), 2139–2153. https://doi.org/10.1175/1520-0442(1999)012<2139:ASOPIT>2.0.CO;2

Liu, Y., Xue, Y., Li, Q., Lettenmaier, D., & Zhao, P. (2020). Investigation of the variability of near-surface temperature anomaly and its causes over the Tibetan Plateau. *Journal of Geophysical Research: Atmospheres*, *125*(19), e2020JD032800. https://doi.org/10.1029/2020JD032800

Lorenz, E. N. (1969). Three approaches to atmospheric predictability. *Bulletin of the American Meteorological Society*, *50*(5), 345–349. https://doi.org/10.1175/1520-0477-50.5.345

Ma, J., Yang, S., & Wang, Z. (2018). Influence of spring soil moisture anomaly in the Indo-China Peninsula on the establishment and development of Asian tropical summer monsoon (in Chinese). *Meteorological and Environmental Sciences*, *41*, 19–30.

Mahanama, S. P. P., Koster, R. D., Reichle, R. H., & Suarez, M. J. (2008). Impact of subsurface temperature variability on surface air temperature variability: An AGCM study. *Journal of Hydrometeorology*, *9*(4), 804–815. https://doi.org/10.1175/2008JHM949.1

Mariotti, A., Ruti, P. M., & Rixen, M. (2018). Progress in subseasonal to seasonal prediction through a joint weather and climate community effort. *npj Climate and Atmospheric Science*, *1*(1), 4. https://doi.org/10.1038/s41612-018-0014-z

Muñoz Sabater, J. (2019). ERA5-Land monthly averaged data from 1950 to present [Dataset]. *Copernicus Climate Change Service (C3S) Climate Data Store (CDS)*. https://doi.org/10.24381/cds.68d2bb30

Niu, G. Y., Yang, Z. L., Dickinson, R. E., & Gulden, L. E. (2005). A simple TOPMODEL-based runoff parameterization (SIMTOP) for use in global climate models. *Journal of Geophysical Research*, *110*(D21). https://doi.org/10.1029/2005JD006111

Oleson, K., Lawrence, D. M., Bonan, G. B., Drewniak, B., Huang, M., Koven, C. D., et al. (2013). *Technical description of version 4.5 of the Community Land Model (CLM), NCAR technical Note NCAR/TN-503+STR* (p. 434). National Center for Atmospheric Research.

Qiu, Y., Feng, J., Wang, J., Xue, Y., & Xu, Z. (2021). Memory of land surface and subsurface temperature (LST/SUBT) initial anomalies over Tibetan Plateau in different land models. *Climate Dynamics*, *62*(4), 1–16. https://doi.org/10.1007/s00382-021-05937-z

Schaefer, K. M., Zhang, T., Tans, P. P., & Stöckli, R. (2007). Temperature anomaly reemergence in seasonally frozen soils. *Journal of Geophysical Research*, *112*(D20), D20102. https://doi.org/10.1029/2007JD008630

Seneviratne, S., Lüthi, D., Litschi, M., & Schar, C. (2006). Land–atmosphere coupling and climate change in Europe. *Nature*, *443*(7108), 205–209. https://doi.org/10.1038/nature05095

Sivapalan, M., Beven, K., & Wood, E. F. (1987). On hydrologic similarity: 2. A scaled model of storm runoff production. *Water Resources Research*, *23*(12), 2266–2278. https://doi.org/10.1029/WR023i012p02266

Song, Y., Chen, H., Wang, L., Huang, A., Gu, W., & Ma, Y. (2023). Soil temperature controls the month-to-month lead-lag correlations of near-surface air temperatures in the middle and lower reaches of the Yangtze River basin. *Journal of Geophysical Research: Atmospheres*, *128*(23), e2023JD039036. https://doi.org/10.1029/2023JD039036

Song, Y., Huang, A., & Chen, H. (2022a). The persistence and reemergence of atmospheric anomaly signals in soil temperature. *Journal of Geophysical Research: Atmospheres*, *127*(19), e2022JD037218. https://doi.org/10.1029/2022JD037218

Song, Y., Huang, A., & Chen, H. (2022b). The storage of antecedent precipitation and air temperature signals in soil temperature over China. *Journal of Hydrometeorology*, *23*(3), 377–388. https://doi.org/10.1175/JHM-D-21.0126.1

Song, Y. M., Wang, Z. F., Qi, L. L., & Huang, A. N. (2019). Soil moisture memory and its effect on the surface water and heat fluxes on seasonal and interannual time scales. *Journal of Geophysical Research: Atmosphere*, *24*(20), 10730–10741. https://doi.org/10.1029/2019JD030893

Tang, M., Wang, J., & Zhang, J. (1987). A primary method for predicting the spring rainfall by the winter soil temperature depth 80 Cm (in Chinese). *Plateau Meteorology*, *6*, 244–255.

Vinnikov, K. Y., Robock, A., Speranskaya, N. A., & Schlosser, C. A. (1996). Scales of temporal and spatial variability of midlatitude soil moisture. *Journal of Geophysical Research: Atmosphere*, *101*(D3), 7163–7174. https://doi.org/10.1029/95JD02753

Wang, Y. H., Chen, W., Zhang, J. Y., & Nath, D. (2013). Relationship between soil temperature in May over Northwest China and the East Asian summer monsoon precipitation. *Acta Meteorologica Sinica*, *27*(5), 716–724. https://doi.org/10.1007/s13351-013-0505-0

Wu, W., & Dickinson, R. E. (2004). Time scales of layered soil moisture memory in the context of land–atmosphere interaction. *Journal of Climate*, *17*(14), 2752–2764. https://doi.org/10.1175/1520-0442(2004)017<2752:TSOLSM>2.0.CO;2

Xue, Y., Diallo, I., Li, W., David Neelin, J., Chu, P. C., Vasic, R., et al. (2018). Spring land surface and subsurface temperature anomalies and subsequent downstream late spring-summer droughts/floods in North America and East Asia. *Journal of Geophysical Research: Atmospheres*, *123*(10), 5001–5019. https://doi.org/10.1029/2017JD028246

Yang, J., Chen, H., Song, Y., Zhu, S., Zhou, B., & Zhang, J. (2021). Atmospheric circumglobal teleconnection triggered by spring land thermal anomalies over West Asia and its possible impacts on early summer climate over North China. *Journal of Climate*, *34*, 5999–6021. https://doi.org/10.1175/JCLI-D-20-0911.1

Yang, K., & Zhang, J. (2016). Spatiotemporal characteristics of soil temperature memory in China from observation. *Theoretical and Applied Climatology*, *126*(3–4), 739–749. https://doi.org/10.1007/s00704-015-1613-9

Yang, Z., & Dominguez, F. (2019). Investigating land surface effects on the moisture transport over South America with a Moisture Tagging Model. *Journal of Climate*, *32*(19), 6627–6644. https://doi.org/10.1175/JCLI-D-18-0700.1

Yang, Z., Zhang, J., Liu, Y., & Li, K. (2022). The substantial role of May soil temperature over Central Asia for summer surface air temperature variation and prediction over Northeastern China. *Climate Dynamics*, *62*(4), 1–15. https://doi.org/10.1007/s00382-022-06360-8

Yang, Z., Zhang, J., & Wu, L. (2019). Spring soil temperature as a predictor of summer heatwaves over northwestern China. *Atmospheric Science Letters*, *20*(3), e887. https://doi.org/10.1002/asl.887

Zhang, J., Yang, Z., & Wu, L. (2018). Skillful prediction of hot temperature extremes over the source region of ancient silk road. *Scientific Reports*, *8*(1), 6677. https://doi.org/10.1038/s41598-018-25063-x

Zhang, Y. R., Shang, G. F., Leng, P., Ma, C., Ma, J., Zhang, X., & Li, Z. L. (2023). Estimation of quasi-full spatial coverage soil moisture with fine resolution in China from the combined use of ERA5-Land reanalysis and TRIMS land surface temperature product. *Agricultural Water Management*, *275*, 107990. https://doi.org/10.1016/j.agwat.2022.107990

Zhu, S., Qi, Y., Chen, H., Gao, C., Zhou, B., Zhang, J., & Wei, J. (2021). Distinct impacts of spring soil moisture over the Indo-China Peninsula on summer precipitation in the Yangtze River basin under different SST backgrounds. *Climate Dynamics*, *56*(5–6), 1895–1918. https://doi.org/10.1007/s00382-020-05567-x